Heat Transfer Modeling of Roller Hearth and Muffle Furnace

by

Kamalpreet Singh Jhajj

A thesis
presented to the University of Waterloo
in fulfillment of the
thesis requirement for the degree of
Master of Applied Science
in
Mechanical Engineering

Waterloo, Ontario, Canada, 2015

AUTHOR'S DECLARATION

I hereby declare that I am the sole author of this thesis. This is a true copy of the thesis, including any required final revisions, as accepted by my examiners.

I understand that my thesis may be made electronically available to the public.

Abstract

In hot forming die quenching, furnaces are used to austenitize ultra high strength steel blanks. In the case of coated steels, like Usibor® 1500 P, furnace heating also transforms a protective Al-Si layer into a permanent Al-Si-Fe intermetallic coating. Modeling this process requires knowledge of the thermophysical properties of the material, specifically, radiative properties and how the sensible energy and latent heat of austenitization change with blank temperature. While the sensible energy is known, there is considerable uncertainty regarding the radiative properties and the latent heat of austenitization.

In this work the effective specific heat of Usibor® 1500 P is inferred through inverse analysis of temperature data collected on coupons heated in a muffle furnace. This technique is first used to validate the heat transfer model, and then used to reveal the distribution of latent heat of austenitization at higher temperatures. The characterization of the radiative properties is carried out on Gleeble-heated coupons using a near-infrared spectrometer and a Fourier transform infrared reflectometer.

Obtained thermophysical properties are employed in developing a heat transfer model for the patched blanks to gain insight into the non-uniform heating of patched blanks. The thermocouple measurements carried out in muffle and roller hearth furnaces are used to validate the modeled temperatures. Various strategies to optimize the heating process for patched blanks are proposed and evaluated, including the use of a high emissivity coating to compensate for the increased thermal mass of the patch.

Acknowledgements

I would first like to thank my supervisor, Dr. Kyle Daun, for his continuous support and encouragement throughout this research. Working with him has been a rewarding experience.

I would also like to express my gratitude to Dr. Mary Wells for her advice and help throughout the course of this study.

I would also like to thank Dave Crigger, Stan Slezak, John Gustin, and Adam Matos of Formet Industries and Nick Adam and Cyrus Yao from Promatek Research Centre for their valuable advice and assistance with furnace experiments.

I would also like to thank my colleagues Noel Chester, Cangji Shi, Josh Rasera, and Jeff Hou for all their assistance and guidance with this research.

Finally, I would like to thank my friends and family for their never-ending support.

Table of Contents

AUTHOR'S DECLARATION ii
Abstract iii
Acknowledgements iv
Table of Contents v
List of Figures vii
List of Tables x
Nomenclature xi
Chapter 1 Introduction 1
1.1 Hot Forming Die Quenching 1
1.1.1 Heat Treatment 2
1.1.2 Blank Transfer 3
1.1.3 Quenching/Forming 3
1.2 Usibor® 1500 P 4
1.3 Motivation 6
1.4 Thesis Outline 7
Chapter 2 Furnace Geometry and Operating Parameters 9
2.1 Roller Hearth Furnace 9
2.1.1 Furnace Geometry 9
2.1.2 Control Strategy 10
2.1.3 Roller Hearth Furnace Characterization 11
2.1.4 Blank Trials 13
2.2 Muffle Furnace 14
2.2.1 Furnace Geometry and Control Strategy 14
2.2.2 Blank Trails 14
2.2.3 Furnace Instrumentation 16
Chapter 3 Heat Transfer Model of Muffle Furnace 18
3.1 Formation and Solution of Governing Equations 18
3.2 Nominal Thermophysical Properties of Usibor® 1500 P 20
3.3 Model Validation up to 500°C 24
3.4 Characterization of Thermophysical Properties of Usibor® 1500 P 27
3.4.1 Latent Heat of Austenitization 27

3.4.2 Characterization of Radiative Properties of Usibor® 1500 P 31
Chapter 4 Heat Transfer Model of Patched Blanks 35
4.1 Blank Discretization 35
4.2 Governing Equations 36
4.3 Model Validation 38
4.3.1 Muffle Furnace 38
4.3.2 Roller Hearth Furnace 39
4.4 Uniform Patch Heating Through Tailored Radiative Properties 41
Chapter 5 Conclusion and Future Work 45
5.1 Conclusions 45
5.2 Future Work 46
Bibliography 48
Appendix A Sensitivity Analysis 51

List of Figures

Figure 1: Components produced using HFDQ. [4] 1
Figure 2: Two variations of HFDQ process: a) direct hot stamping b) indirect hot stamping. [3] 2
Figure 3: Roller hearth furnace located at Formet Industries. 3
Figure 4: Continuous cooling transformation diagram of 22MnB5 steel [13]. 6
Figure 5: Schematic drawing of a roller hearth furnace, highlighting radiant tubes, baffles and rollers. 10
Figure 6: (a) Shows full length of a radiant tube, (b) thermocouple installation on top of radiant tube with ceramic paste, and (c) placement of additional K-Type thermocouples on the side wall. 12
Figure 7: Temperature measurements made in zone 2 of the roller hearth furnace. 13
Figure 8: Measured temperature histories of blanks heated in the roller hearth furnace..... 14
Figure 9: Setup for thermocouple measurements conducted in the muffle furnace on unpatched blanks (left) patched blank (right)..... 16
Figure 10: Thermocouple measurements of unpatched (left) and patched (right) blanks heated in the muffle furnace. 16
Figure 11: Temperature variation within the muffle furnace during blank heating. 17
Figure 12: Shows the control volume of an unpatched blank used to derive the heat transfer model along with relevant boundary conditions..... 19
Figure 13: Twynstra et al. [6] modified the specific heat provided by the manufacturer [19] by assuming that the latent heat is distributed uniformly between T_{Ac1} and T_{Ac3}. Tonne et al. [23] inferred $c_{p,eff}$ through nonlinear regression of modeled data to thermocouple data collected in a roller hearth furnace. 22
Figure 14: (a) Spectral emissivity of Usibor® 1500 P provided by the manufacturer [19]; (b) total emissivity and absorptivity calculated based on the provided spectral emissivity measurements. 23
Figure 15: Schematic of first-order Tikhonov regularization using the L-curve. Plots (a), (b), and (c) show temperature heating rates obtained using insufficient, optimal, and excessive regularization. .. 25
Figure 16: Specific heat of Usibor® 1500 P inferred from low temperature muffle furnace experiments. Dashed curves indicate individual measurements, solid curves indicate averages, and shaded regions indicate uncertainty associated with T_{surr}..... 27
Figure 17: (a) Spectral emissivity of BN-coated 22MnB5; (b) total emissivity and absorptivity. 28
Figure 18: Effective specific heats for 22MnB5 at high temperatures. Present values are obtained from temperature measurements on BN-coated 22MnB5 blanks within the muffle furnace, using Eq.

(8) to find T_{surr}. The shaded region indicates uncertainty in c_p due to uncertainty in T_{surr}. Other curves are as labeled in Figure 13. 29
Figure 19: Comparison of Gleeble power angle with $c_{p,eff}$ inferred from muffle furnace measurements. 30
Figure 20: Modeled $c_{p,eff}$ assuming that the latent heat of austenitization is absorbed according to a triangular profile between T_{Ac1} and T_{Ac3}. The shaded areas correspond to the latent heat of austenitization of 22MnB5, 85 kJ/kg [30]. 31
Figure 21: Spectral emissivity measurements carried out using NIR spectrometer (0.9 to 2.5μm) and FTIR reflectometer (2 to 25 μm)..... 32
Figure 22: Total emissivity and total absorptivity based on the new measurements. 33
Figure 23: Inferred effective specific heat calculated using Eq. (5) and radiative properties presented in Figure 14 and Figure 22. 34
Figure 24: Geometry simplifications of a) B-pillar, b) hinge pillar, and c) bumper blanks. Discretized geometry along with conduction to an internal volume element is shown in d) and e) respectively... 36
Figure 25: Comparison of modeled and measured (a) temperature histories (b) heating rates for patched blanks heated within the muffle furnace. (Solid and dashed lines denote measurements and modeled results, respectively.)..... 39
Figure 26: Comparison of modeled and measured (a) temperature histories (b) heating rates for patched blanks heated within the roller hearth furnace. (Solid and dashed lines denote measurements and modeled results, respectively.)..... 41
Figure 27: (a) Modeled and measured temperatures for patched blanks with a boron nitride coating on the patch heated within muffle furnace (b) heating rates of modeled and measured temperature with boron nitride coated patch. (Solid and dashed lines denote measurements and modeled results, respectively.)..... 42
Figure 28: (a) Modeled and measured temperatures for patched blanks with a boron nitride coating on the patch heated within roller hearth furnace (b) heating rates of modeled and measured temperature with boron nitride coated patch. (Solid and dashed lines denote measurements and modeled results, respectively.)..... 43
Figure 29: Growth of intermetallic Al-Si-Fe layer in a boron nitride coated patched blank heated in the muffle furnace. 44

Figure 30: Shows modeled temperature range calculated based on the upper and lower limits of surrounding temperature in each zone. 52
Figure 31: Shows the modeled temperature of the boron nitride coated hinge pillar patch with different air gap thicknesses. 53
Figure 32: Shows the modeled temperature of the bumper (1.3mm) and hinge pillar (2.6mm) blanks with α at 575°C set to 0.15, 0.2 and 0.25. (Solid lines show the modeled temperature with α set to 0.2 and dashed lines show the modeled temperature with α set to 0.15 and 0.25) 53

List of Tables

Table 1: Summary of the chemical composition of 22MnB5 steel [13]. 4
Table 2: Mechanical properties of 22MnB5 steel [13]. 5
Table 3: Summary of zone temperature set-points of the roller hearth furnace located at Formet Industries. 11
Table 4: Dimensions of blanks used in thermocouple measurements in roller hearth furnace. 13
Table 5: Temperature dependent properties of Usibor® 1500 P. 21
Table 6: Required heating time to reach 900°C for blanks heated in roller heart furnace. 40

Nomenclature

Symbol	Units	Definition
T_{surr}	$°C$	Surrounding temperature
T_s	$°C$	Blank temperature
T_∞	$°C$	Ambient temperature
T_{sub}	$°C$	Substrate blank temperature
T_f	$°C$	Film temperature
T_i^k	$°C$	Temperature of *ith* element at *kth* iteration
h_{top}/h_{bottom}	$W/(m^2.°C)$	Convection coefficient
$Nu_{L,top}/Nu_{L,bottom}$		Nusselt number
Ra_L		Rayleigh number
Pr		Prandtl number
U	$W/(m^2°C)$	Overall heat transfer coefficient between patch and substrate blank
L	m	Characteristic length of the blank
A_s	m^2	Total surface area (top and bottom)
A_i	m^2	Total exposed surface area (top and bottom) of *ith* element
$A_{i,top}/A_{i,bottom}$	m^2	Exposed surface area of the top/bottom *ith* element
w	m	Thickness of blank
t_{gap}	m	Air gap between patch and substrate blank
V	m^3	Volume
$\Delta x, \Delta y$	m	Length and width of volume element

ρ	kg/m^3	Density of Usibor® 1500 P
$c_{p,eff}$	$J/(kg.K)$	Effective specific heat of Usibor® 1500 P
α, α_λ		Absorbtivity of Usibor® 1500 P
ε, ε_λ		Emissivity of Usibor® 1500 P
k, k_{air}	$W/(m.K)$	Thermal conductivity
β	$°C^{-1}$	Volume expansion coefficient
α	m^2/s	Thermal diffusivity
v	m^2/s	Kinematic viscosity
$\dot{Q}_{net,\mathrm{rad},i}$	W	Net radiation heat transfer to the *ith* volume element
$\dot{Q}_{net,conv,i}$	W	Net convection heat transfer to the *ith* volume element
$\dot{Q}_{net,cond,i}$	W	Net conduction heat transfer to the *ith* volume element
$\mathfrak{F}_{i-s}$		Radiation exchange factor between surface *i* and *s*
Δt	s	Time step
g	m/s^2	Acceleration due to gravity
σ	$W/(m^2.K4)$	Stefan-Boltzmann constant

Chapter 1
Introduction

1.1 Hot Forming Die Quenching

Hot forming die quenching (HFDQ), also known as hot stamping, is a manufacturing process used in the automotive industry to produce lighter car components with high strength and improved crash performance. In the last few decades, components manufactured using hot forming die quenching have increased significantly from 3 million in 1987 to an estimated 450 million in 2015 [1] [2] due to the consistent demand of lighter vehicles with improved safety and crashworthiness [3]. Chassis components such as A-pillar, B-pillar, bumper, roof rail, rocker rail and tunnel, shown in Figure 1, are commonly produced using HFDQ [3].

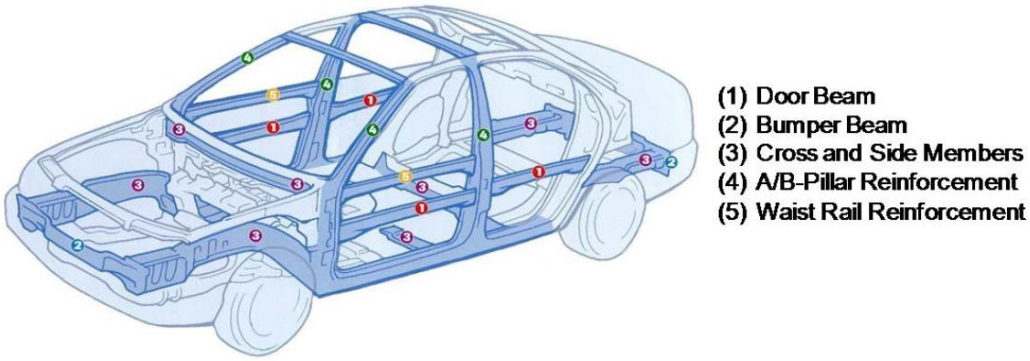

Figure 1: Components produced using HFDQ. [4]

Hot forming die quenching consists of three steps: 1) heat treatment of steel sheets; 2) transfer of steel sheets to forming die; and 3) simultaneous quenching and forming of steel sheets. Direct and indirect hot forming are two variations of this general process that are common to the manufacturing industry. In direct hot forming, steel sheets are heated in a furnace and then transferred to a die for simultaneous quenching and forming. However, in indirect hot forming, steel sheets are nearly formed to the desired shape using cold forming techniques and these cold formed parts are heated in a furnace and then quenched and pressed to the final shape in the die. These two variations of the HFDQ are highlighted in Figure 2.

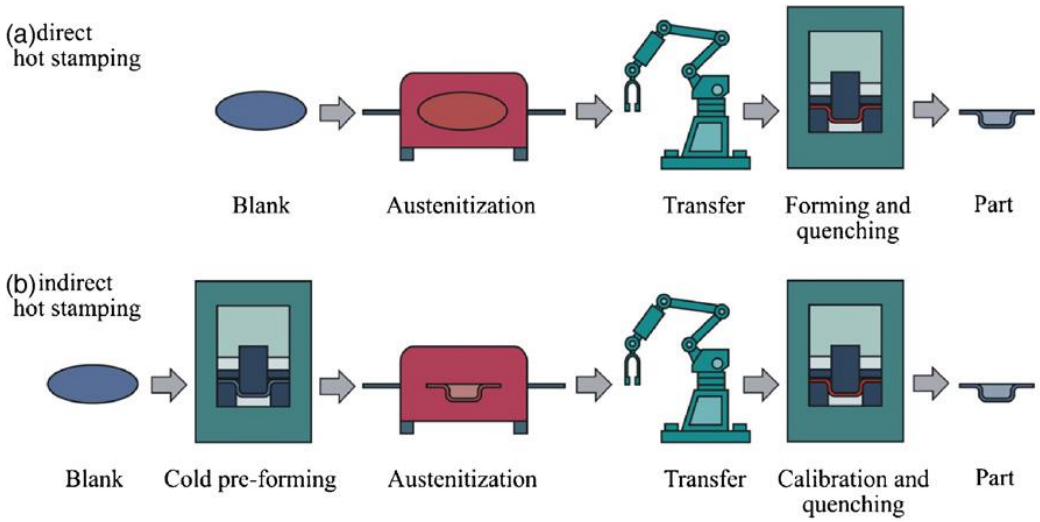

Figure 2: Two variations of HFDQ process: a) direct hot stamping b) indirect hot stamping. [3]

1.1.1 Heat Treatment

The main objective of heat treatment in HFDQ is to transform the ferrite and pearlite phases present in the as-received steel blanks into the ductile austenite phase that can be easily formed into the desired shape. Additionally, for coated steels, such as Usibor® 1500P, it is also desirable to transform the Al-Si coating into an Al-Si-Fe intermetallic layer that has corrosion resistance properties. Temperatures at which the austenitization of steel begins and ends (T_{Ac1} and T_{Ac3}, respectively) are directly influenced by the carbon content of the steel and other alloying elements. It is necessary for the blank to be completely austenitized before forming/quenching in order to achieve a fully martensitic microstructure needed to obtain the desired strength and hardness in the formed part.

The majority of HFDQ lines use indirect-fired roller hearth furnaces, like the one shown in Figure 3, to heat treat blanks [5]. (Alternative heating strategies like batch furnaces [6], direct contact heating [7] [8] [9], and die induction heating [10], are under development but limited in application [3].) Roller hearth furnaces are typically 20-30 m long and are heated with natural-gas fired radiant tubes. The furnace is divided into several zones, each with its own controlled set-point temperature. Blanks are conveyed through the zones via rotating ceramic rollers and are heated by thermal radiation from the furnace surroundings, convection from the furnace atmosphere, and conduction from the rollers. Blanks of varying shapes and thicknesses are used to produce a wide range of automotive components [4], and depending on its mass, each blank type must be heat-treated at a

specific rate to obtain adequate austenitization. Inadequate heating leads to incomplete austenitization, which in turn prevents the as-formed part from having a fully martensitic microstructure.

Figure 3: Roller hearth furnace located at Formet Industries.

1.1.2 Blank Transfer

Blanks are transferred from the furnace to the forming die at the end of the heat treatment process. During the transfer, blanks are at a significantly higher temperature compared to the surroundings, which results in rapid heat loss to the cold surroundings and a decrease in blank temperature. It is necessary to complete the blank transfer from the furnace to the die as fast as possible so that the temperature of the blank at the end of the transfer is not below the T_{Ac3} temperature to avoid the formation of soft ferrite or bainite phases after quenching.

1.1.3 Quenching/Forming

Heated blanks are quenched in a water cooled die to transform the ductile austenite phase into hard martensitic microstructure. The cooling rate required to obtain this transformation depends on the carbon content of the steel and its alloying elements. In most HFDQ processes, the objective is to obtain a uniform cooling rate throughout the blank to minimize variation in the resulting mechanical properties such as yield strength and hardness; however, a variable cooling rate has significant applications in development of tailored blanks [11]. The cooling rate of the blank is influenced by the surface temperature of the die, and, to a lesser extent, the contact pressure between the die and the blank [12]. It is relatively simple to ensure uniform surface temperature of the die by water cooling the die using internal channels within the die. However, controlling the contact pressure between the

die and blank is challenging and depends on the geometry of the blank. As-formed blanks of complex geometries experience variation in mechanical properties due to the non-uniform cooling resulting from non-uniform contact pressure between the die and the blank. Dies are designed to minimize the variation in contact pressure as much as possible and this imposes a limit on the type of parts that can be manufactured using a hot forming die quenching process.

1.2 Usibor® 1500 P

One of the most ubiquitous steels for HFDQ, Usibor® 1500 P, consists of 22MnB5 steel coated with a ~15-30 μm of Al-Si layer (~90% Al by mass) to provide protection against scaling and decarburization during heating. The Al-Si coating melts at 575°C during heating and reacts with iron that diffuses from the substrate steel, forming a corrosion-resistant Al-Si-Fe layer. The thickness of this ternary layer is directly related to the heating time, as longer heating times allow for extended diffusion resulting in thicker layers and vice versa. Consequently, the blank heating rate must be adjusted for adequate growth of the Al-Si-Fe layer as thicker layers reduce the weldability of the blank and thinner layers might not provide sufficient corrosion resistance.

The 22MnB5 steel, along with other boron alloy steels such as 27MnCrB5 and 37MnB4, can produce a fully martensitic microstructure upon quenching [13] hence they are widely used in HFDQ. The 22MnB5 steel has low carbon content of 0.23% and the addition of B, Mn and Cr alloying elements influence the hardenability of the formed part [3]. The chemical composition of 22MnB5 steel is summarized in Table 1.

Table 1: Summary of the chemical composition of 22MnB5 steel [13].

Steel	Al	B	C	Cr	Mn	N	Ni	Si	Ti
22MnB5	0.03	0.002	0.23	0.16	1.18	0.005	0.12	0.22	0.040

The microstructure of as-received samples of 22MnB5 steel contains approximately 75% ferrite and 25% pearlite; phase transformation from ferrite/pearlite to austenite begins at 720°C and is completed at 880°C as summarized in Table 2. That being said, austenitization is not instantaneous, but rather depends on time; thus blanks heated rapidly to the T_{Ac3} temperature (880°C) might require additional soak time at or above the T_{Ac3} temperature to be completely austenitized [14]. In contrast, Garcia and Deardo [15] investigated austenite formation kinetics in a 1.5% Mn steel with comparable carbon content to 22MnB5 and obtained full austenitization by holding coupons at 725°C for several

hours. This highlights that the austentization process is not strictly dependent on temperature only as it also has weak time dependence as well. In a roller hearth furnace, the heating rate is slow enough that the blank is completely austenitized upon reaching the T_{Ac3} temperature and does not require any additional soak time in the furnace.

Table 2: Mechanical properties of 22MnB5 steel [13].

T_{Ac1} [°C]		720
T_{Ac3} [°C]		880
M_s [°C]		425
M_f [°C]		280
Critical Cooling rate [°C /s]		27
Yield Stress [MPa]	As-received	457
	Hot Stamped	1010
Tensile Strength [MPa]	As-received	608
	Hot Stamped	1478

The continuous cooling transformation (CCT) diagram of 22MnB5 steel shown in Figure 4 can be used to estimate the critical cooling rate required to transform austenite into martensite. The transformation from austenite to martensite begins at 425°C and is completed at 280°C and the critical cooling rate necessary to obtain this transformation is 27 °C/s for 22MnB5 steel. If the cooling rate is lower than the critical cooling rate then some of the austenite will transform into bainite, ferrite and/or pearlite with lower hardness as shown in the Figure 4. Fully martenisitic 22MnB5 steel has a hardness of approximately 500 HV and a yield stress and tensile strength of 1000 MPa and 1500 MPa, respectively.

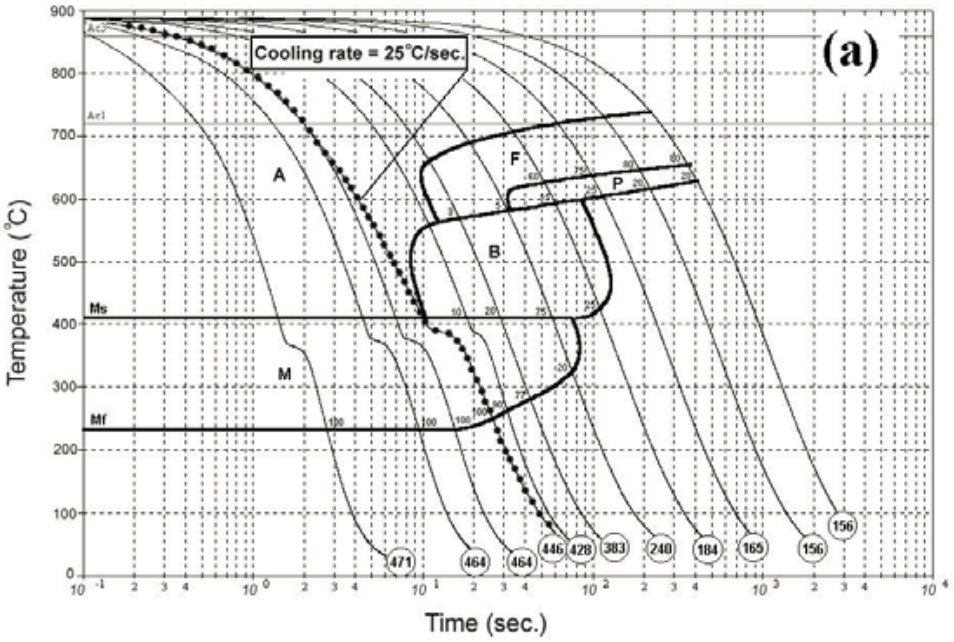

Figure 4: Continuous cooling transformation diagram of 22MnB5 steel [13].

1.3 Motivation

Cosma International, a Tier I auto parts manufacturer, leads Canada's automotive industry in hot forming die quenching (HFDQ). Most of the HFDQ lines at Cosma use roller hearth furnaces for the heat treatment of the blanks. Understandably, it is in Cosma's best interest to operate these furnaces efficiently to improve the production rate and to minimize the energy consumption while ensuring complete austenitization of blanks and adequate growth of the Al-Si-Fe layer in Usibor® 1500 P blanks. In roller hearth furnaces, it is a common practice to simultaneously heat blanks of varying geometry and thicknesses in order to increase the throughput of the furnace; however, due to the variation in thickness and geometry, each blank must pass through the furnace at a certain rate (or, equivalently, be heated for a certain duration) in order to avoid incomplete austenitization of the blank. Shorter heating times might result in incomplete austenitization whereas longer heating times result in excess Al-Si-Fe layer growth, which impacts the weldability of as-formed components [3]. Patched blanks, in which a small patch is spot-welded to the substrate blank to locally-enhance the crash performance of the blank, are particularly susceptible to incomplete austenitization and non-uniform heating in roller hearth furnaces. The added thermal mass of the patch requires longer

heating time and causes non-uniform heating within the blank which results in non-uniform growth of Al-Si-Fe layer.

Currently, furnace parameters such as roller speed and zone temperature are adjusted by a trial-and-error process to accommodate blanks of different thicknesses and geometries. This is a time consuming process that must be repeated whenever there is a change in the blank geometry or thickness; this makes it difficult to optimize furnace parameters without understanding the heat transfer and metallurgical processes occurring within the furnace, and results in considerable material waste before a satisfactory set of parameters is identified. The objective of this research is to develop a heat transfer model of the furnace capable of predicting blank temperature, which will be used to adjust the furnace operating parameters (roller speed and zone temperature) to accommodate varying blank geometries and thicknesses. The model will also be used to identify reasons for incomplete austenitization and non-uniform heating in patched blanks, form the basis of an algorithm for optimizing the heating process.

1.4 Thesis Outline

The thesis is divided into five main sections: discussion of furnace geometry and operational parameters; presentation of the heat transfer model developed for muffle furnace along with the characterization of thermophysical properties of Usibor® 1500 P; development and validation of the heat transfer model for patched blanks; and a summary of the presented work with conclusions.

Chapter 2 will present information regarding the types of furnaces involved in this study. First physical attributes of the furnaces will be discussed, including geometrical dimensions, control strategies, and temperature set-points. Next, instrumentation methodologies employed for each type of furnaces are discussed along with the experimental results.

Chapter 3 focuses on the development of the heat transfer model for the muffle furnace and characterization of thermophysical properties of Usibor® 1500P. In particular, the heat transfer model is used to infer the distribution of the latent heat of austenitization by heating boron nitride coated samples in the muffle furnace. This chapter concludes with the results from the characterization of temperature dependent radiative properties of Usibor® 1500P.

Chapter 4 will extend the model developed in Chapter 3 to predict the transient temperature of patched blanks heated in muffle and roller hearth furnaces. The validation of the model is carried out using the experimental results presented in Chapter 2 for both patched and unpatched blanks. This

chapter concludes by evaluating the effectiveness of high absorbing coatings to obtain uniform heating within patched blanks.

Finally, Chapter 5 will summarize the presented work along with the recommendations and future work.

Chapter 2
Furnace Geometry and Operating Parameters

Two types of furnaces were involved in this study: an industrial size roller hearth furnace and lab scale muffle furnace. The roller hearth furnace, manufactured by Schwartz GBMH, is located at Formet Industries in St. Thomas, Ontario, whereas the smaller muffle furnace, manufactured by Thermolyne, is located at University of Waterloo. The muffle furnace operating temperature was set to recreate the heating rates similar to those observed in the roller hearth furnace, and was extensively characterized, as described below. The more controlled environment of the muffle furnace is better suited to characterize thermophysical properties of Usibor® 1500 P blanks and to validate the preliminary furnace heat transfer model. Moreover, the cost of carrying out experiments in the roller hearth furnace is significantly higher than the muffle furnace as it requires stopping production and uses more material and thermocouple wires. Therefore, most of the experiments in this study were carried out in the muffle furnace to develop a heat transfer model of the muffle furnace, which was later extended to the roller hearth furnace. The roller hearth furnace tests, used to characterize the industrial process, and to validate the final heat transfer model, were carried out with the help of Formet personnel.

2.1 Roller Hearth Furnace

2.1.1 Furnace Geometry

The roller hearth furnace is an industrial furnace that is used to austenitize blanks in the hot stamping die quenching process. It is approximately 30 m long and 2 m wide. The furnace is divided into 12 zones, some of which are thermally-isolated from each other by baffles as shown in Figure 5. Blanks are conveyed through the furnace on uniformly spaced ceramic rollers while being irradiated from the top and bottom via natural gas fired radiant tubes, which indirectly heat the blanks without contaminating the blank surface with combustion gases. For the initial 15m of the furnace, radiant tubes are located at both the top and bottom of the furnace; however, for the last 15m of the furnace, the radiant tubes are located only at the top of the furnace. The average distance between two consecutive radiant tubes is approximately 1.35 m; however, radiant tubes are more closely spaced at the beginning of the furnace compared to the end of the furnace.

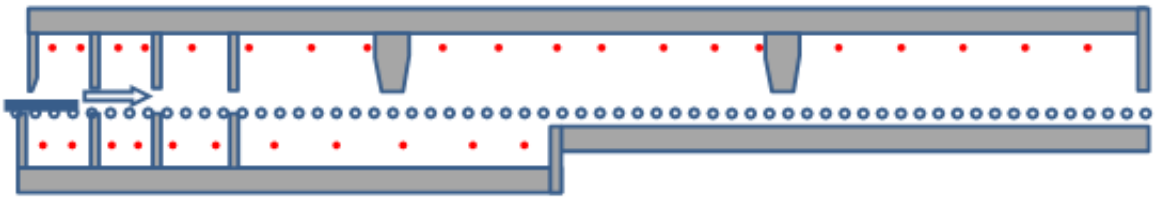

Figure 5: Schematic drawing of a roller hearth furnace, highlighting radiant tubes, baffles and rollers.

2.1.2 Control Strategy

The roller hearth furnace at Formet Industries is used to heat treat blanks of various geometries and thicknesses such as b-pillars, hinge pillars and bumpers. The thicknesses of these blanks vary from 1 mm to 3 mm (patched thickness) and as a result of this variation, the heating time of blanks vary from 3 to 8 minutes. The temperature set-points of each zone are adjusted by trial-and-error to develop a generic temperature profile within the furnace that can be applied to blanks with different geometries and thicknesses. The zone temperature is controlled by grounded K-type thermocouples suspended within the furnace; the fuel supply to the radiant tubes within the zone is turned on or off whenever the measured temperature exceeds an upper and lower bound (typically ±20 °C) surrounding the set-point temperature, via a hysteresis "bang-bang" control strategy.

The set-point temperature of furnace zones is not varied between blanks with different geometry and thicknesses; instead changes to the blank heating rate are realized by varying the roller speed. Table 3 shows the set-point temperature of each zone of the roller hearth furnace located at Formet Industries. In this study, experiments involving the roller hearth furnace were performed using this particular furnace.

Table 3: Summary of zone temperature set-points of the roller hearth furnace located at Formet Industries.

Zone	Temperature Set-point [°C]
1	875
2	875
3	875
4	900
5	900
6	925
7	925
8	930
9	935
10	935
11	935
12	935

2.1.3 Roller Hearth Furnace Characterization

As mentioned in the previous section, the temperature of each zone of the roller hearth furnace is controlled using a K-type thermocouple that is installed on a side wall approximately halfway between the ceramic rollers and the ceiling of the furnace. In order to better characterize the furnace temperature, University of Waterloo personnel were invited to install additional sensors during scheduled furnace maintenance. An additional 15 K-type thermocouples were installed in three zones of the furnace (zones 2, 7, and 11, five thermocouples per zone) in order to capture any temperature variation within a zone and to obtain a more detailed temperature profile of the furnace. Within each zone, two thermocouples were installed on the surface of the radiant tube as shown in Figure 6, one at each end of the tube. One thermocouple was installed on the surface of the insulation of the side wall of the furnace while one grounded and one ungrounded thermocouples were used to measure the air temperature of the furnace.

(a) (b)) (c)

Figure 6: (a) Shows full length of a radiant tube, (b) thermocouple installation on top of radiant tube with ceramic paste, and (c) placement of additional K-Type thermocouples on the side wall.

Results from this furnace instrumentation of zone 2 are presented in Figure 7. As expected, a cyclic trend is observed in the measured temperature, arising from the hysteresis control strategy described above. The surface of the radiant tube is at the highest temperature in the zone and surface of the side wall is at the lowest; the difference in these two temperatures is approximately 10°C. Air temperatures measured using grounded and ungrounded thermocouples are found to be similar throughout the measurement period. The temperature within zone two fluctuates with amplitude of approximately 5-7°C and over a period of 400 seconds; zones located in the middle of the furnace have lower fluctuations in temperature due to lower heat losses in comparison to the zones located at the beginning and end of the furnace. Moreover, fluctuations in zone temperature also depend on the type of blanks that are heated; blanks with more mass will absorb more heat from the furnace, thus resulting in frequent cycling of radiant tube burners.

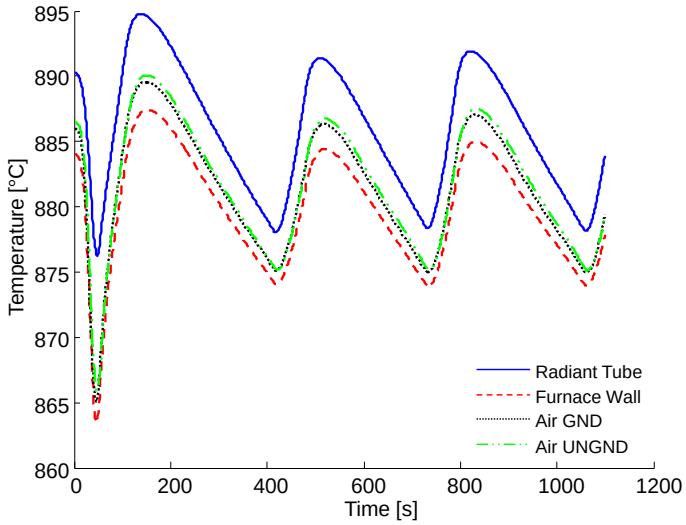

Figure 7: Temperature measurements made in zone 2 of the roller hearth furnace.

2.1.4 Blank Trials

Further insight into roller hearth furnace heating is obtained by measuring the transient temperature of various blanks by attaching thermocouples to the surface of the blanks; recorded temperature data are also used to validate the heat transfer model of the roller hearth furnace, as discussed later in the thesis. Tests were carried out on three types of blanks: B-pillar; hinge pillar; and bumper blanks. Both the B-pillar and hinge pillar blanks are patched blanks, whereas bumper blanks are unpatched. Approximate dimensions along with unpatched and patched thicknesses of the blanks are summarized in Table 4.

Table 4: Dimensions of blanks used in thermocouple measurements in roller hearth furnace.

Blank Type	Thickness [mm] Unpatched/Patched	Dimensions [m]
B-pillar	1.5/3.0	1 × 0.3
Hinge pillar	1.3/2.6	1.5 × 0.5
Bumper	1.3	1.7 × 0.5

A K-type thermocouple was welded to the blank surface and was tied to the blank approximately 150 mm away from the thermocouple junction to provide additional structural support

during the conveying process. Figure 8 shows the temperature histories of B-pillar, hinge pillars and bumper blanks heated in the roller hearth furnace. It can be observed that the bumper blanks reach T_{Ac3} in approximately 200 seconds whereas hinge pillar and B-pillar blanks require 350 and 450 seconds to be completely austenitized, respectively, due to their larger thermal mass. This provides insight into the non-uniform heating experienced in the patched blanks, as the substrate blank (usually 1.3 or 1.5 mm thick) will reach T_{Ac3} approximately 150 – 200 seconds prior to the patched sections.

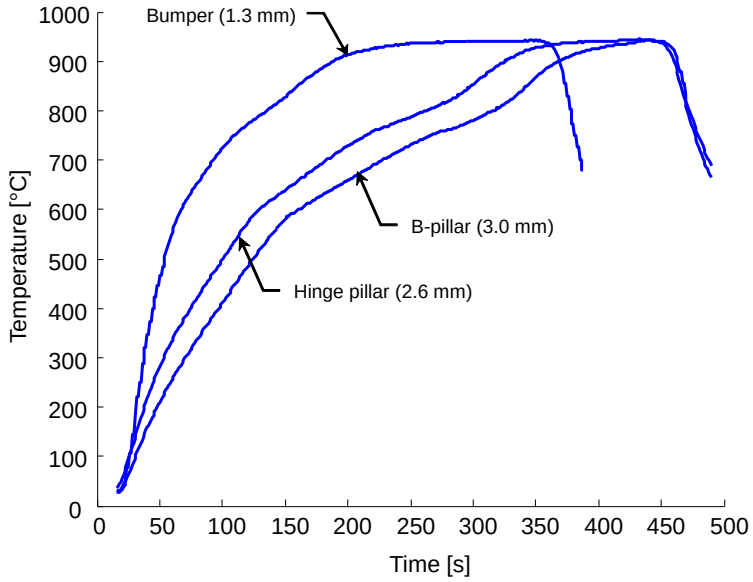

Figure 8: Measured temperature histories of blanks heated in the roller hearth furnace.

2.2 Muffle Furnace

2.2.1 Furnace Geometry and Control Strategy

The muffle furnace is significantly smaller in size compared to the roller hearth furnace, with internal dimensions of 460 × 230 × 230 mm. It is heated via electrical resistance elements embedded in the top and bottom furnace walls. These elements are controlled using one K-type thermocouple and the power to the electrical elements is controlled through a PID controller to maintain the specified temperature within the furnace.

2.2.2 Blank Trails

The muffle furnace was used to recreate the heating rates observed in the roller hearth furnace for both patched and unpatched blanks. Two sets of tests were conducted in the muffle furnace; initially

unpatched blanks were heated to approximately 500°C to validate the preliminary heat transfer model, and a second set of tests consisted of patched blanks heated to austenitization temperatures. This was done to avoid introducing uncertainty in the radiative properties of Usibor® 1500 P upon melting of Al-Si coating, which is discussed in more detail in Chapter 3. Below 500°C, the coating remains inert, and the spectral emissivity (and hence total emissivity and absorptivity) are well-known.

A frame was constructed from RSLE 57 ceramic insulation to provide a platform for the coupons during heating, and to promote consistency between tests. The coupon only contacts the platform at four corners as shown in Figure 9, and the thermocouple is welded at the center of the coupon in order to minimize conduction heat transfer from the platform to the coupon. The unpatched blanks, 127 mm × 127 mm steel blanks of three different thicknesses: 1.3 mm; 1.8 mm; and 2.4 mm, were heated to approximately 500°C. For the patched blanks, substrate blanks with dimensions of 130 mm × 30 mm × 1.3 mm with a spot-welded patch of 50 mm × 30 mm × 1.3 mm were heated to approximately 900°C. As shown in Figure 9, unpatched blanks were instrumented with one K-type thermocouple welded at the center of the blank, whereas patched blanks were instrumented with two K-type thermocouples; one was attached to the patch itself and the other was attached to the substrate blank to measure the difference in heating rates within the blanks. Before each series of tests, the furnace was allowed to soak for at least two hours to ensure that it reached steady state. The temperature histories of unpatched and patched blanks heated in the muffle furnace are shown in Figure 10. Temperature histories obtained from muffle furnace tests are similar to the ones obtained in the roller hearth furnace, however, patched blanks (2.6 mm) heated in the muffle furnace reached austenitization temperature 100 seconds earlier than the 2.4 mm thick patched blanks heated in roller hearth furnace, thus indicating a faster heating rate in the muffle furnace.

Figure 9: Setup for thermocouple measurements conducted in the muffle furnace on unpatched blanks (left) patched blank (right).

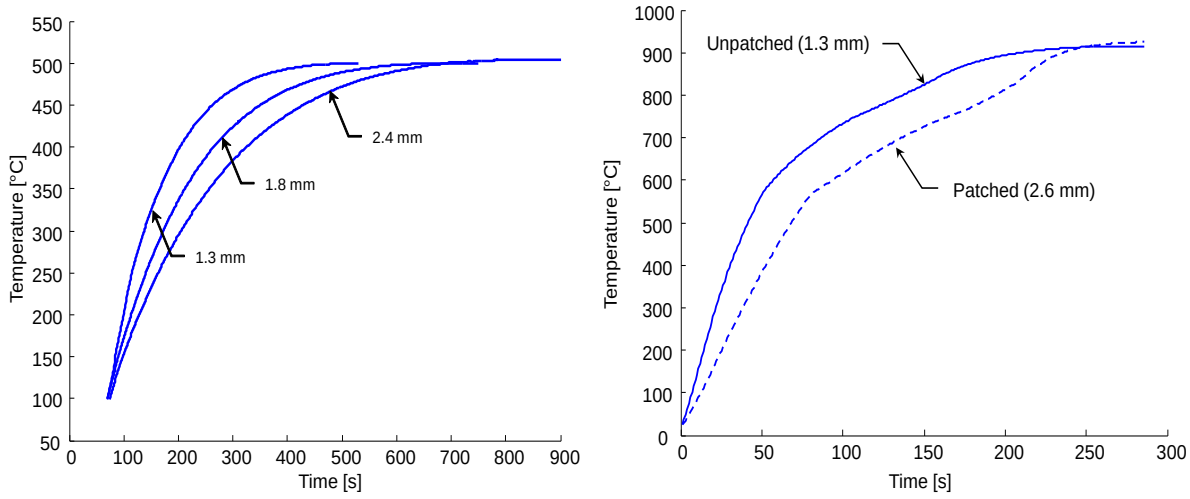

Figure 10: Thermocouple measurements of unpatched (left) and patched (right) blanks heated in the muffle furnace.

2.2.3 Furnace Instrumentation

As stated previously, the temperature of the muffle furnace is controlled by one K-type thermocouple that is suspended near the back of the furnace, but this is clearly inadequate to assess the temperature uniformity within the furnace. Therefore, an additional five K-type thermocouples were installed in the furnace in order to obtain a more accurate temperature profile within the furnace. Three thermocouples were embedded in the surface of the side wall and one thermocouple was embedded in

the inside surface of the door. Another K-type thermocouple was used to measure the air temperature of the furnace and was placed approximately near the center of the furnace. Figure 11 shows the temperature histories obtained from these five thermocouples during a blank heating test. Notably, there is a significant drop in the door temperature of the furnace as the blank is placed in the furnace. The temperature of the furnace door drops from 450°C to 250°C during blank loading while the temperature of the rest of the furnace remains unchanged. Once the blank is placed inside the furnace and the door is closed, it takes the furnace door approximately 50 seconds to thermally equilibrate with the rest of the furnace. This shows that for the first 50 seconds of the heating, the furnace door also acts as a heat sink along with the blank; this might be significant during the development of a heat transfer model of the muffle furnace. Additionally, it can also be observed that the temperature at the center of the furnace is approximately 10°C higher than the temperature at the front and back of the furnace. This indicates that there is a noticeable variation in the temperature of the furnace from the front to the back, most likely due to better insulation of the side walls of the furnace compared to the door and rear wall. During the development of the heat transfer model of the furnace, it may be important to consider the variation in the temperature within the muffle furnace.

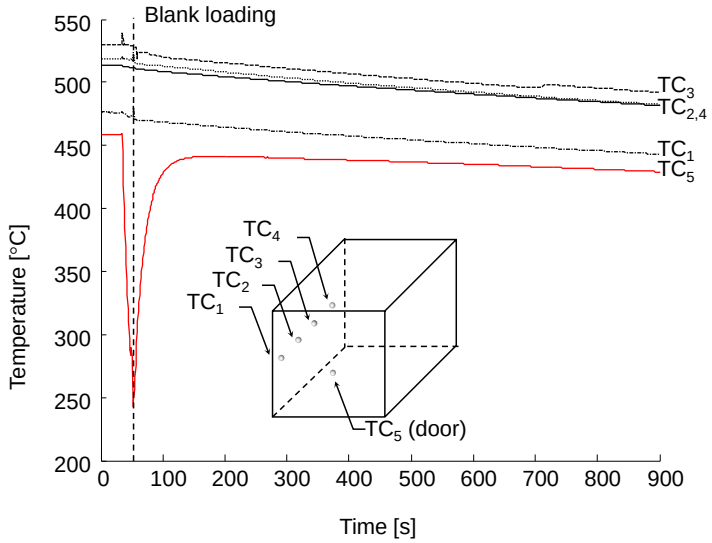

Figure 11: Temperature variation within the muffle furnace during blank heating.

Chapter 3
Heat Transfer Model of Muffle Furnace

The initial heat transfer model was developed for unpatched blanks heated in a muffle furnace according to the experimental setup presented in the previous chapter. The model is based on the following assumptions: (1) radiation and convection are the dominant mode of blank heating, so conduction heat transfer from the ceramic platform can be neglected; (2) the blank is irradiated equally from above and below; (3) the furnace surroundings are large and isothermal; (4) the spectral emissivity of the blank is equal to the spectral absorptivity of the blank; and (5) the edges of the blank are assumed to be adiabatic.

As noted above, there is also some uncertainty regarding the radiative properties of Usibor® 1500P, particularly above 575°C when the Al-Si coating melts and then reacts with iron from the 22MnB5 substrate. Therefore, the initial model is validated for temperatures below the melting point of Al-Si coating using the temperature histories of unpatched blanks from the muffle furnace experiments. Then, the validated model is used to infer the distribution of latent heat of austenitization of Usibor® 1500 P based on experiments conducted at the University of Waterloo. Finally, the changing spectral emissivity of the blank at higher temperatures, assessed through a combination of *in situ* measurements using a Gleeble/NIR spectrometer and *ex situ* measurements made on heated and quenched blanks using a FTIR reflectometer, are incorporated into the model.

3.1 Formation and Solution of Governing Equations

The control volume used to derive the heat transfer model encompasses the entire unpatched blank as shown in Figure 12; the boundary conditions for this control volume based on the assumptions presented above are also shown in this figure. The coupon heating rate can be modeled by

$$\rho c_{p,eff} w \frac{dT_s}{dt} = 2\alpha\sigma T_{surr}^4 - 2\varepsilon\sigma T_s^4(t) + \left(h_{top} + h_{bottom}\right)\left(T_{surr} - T_s\right) \quad (1)$$

where ρ is the density of Usibor® 1500 P, w is the coupon thickness, T_s is the coupon temperature, T_{surr} is the surrounding temperature, t is time, σ is the Stefan-Boltzmann constant, α and ε are the total absorptivity and emissivity of the blank, and h_{top} and h_{bottom} are the average convection coefficients over the upper and lower surfaces of the blank.

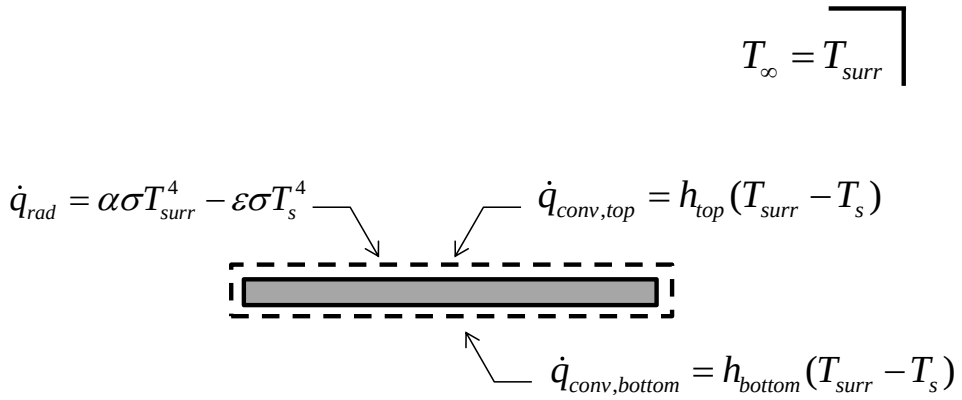

Figure 12: Shows the control volume of an unpatched blank used to derive the heat transfer model along with relevant boundary conditions.

To a good approximation the air within the muffle furnace is quiescent, so convection heat transfer is due to natural convection. The heat transfer coefficient from the top of the blank is found by [16]

$$Nu_{L,top} = \frac{h_{top}L}{k_{air}} = 0.52Ra_L^{1/5} \tag{2}$$

where Ra_L is the Rayleigh number,

$$Ra_L = \frac{g\beta(T_s - T_\infty)L^3}{\alpha\nu} \tag{3}$$

The properties of air (k_{air}, α, ν, $\beta = 1/T_f$) are evaluated at the film temperature, $T_f = 0.5(T_\infty + T_s)$ and T_∞ is taken to be the surrounding temperature, while $L \equiv A/P$, where A and P are the area and perimeter of the blank. For the bottom surface, it is necessary to account for the confinement of the frame walls, which, along with the furnace floor and blank underside, form a narrow cavity. In this scenario we use the correlation of Hollands et al. [17] as reported in [18],

$$Nu_{L,bottom} = \frac{h_{bottom}L}{k_{air}} = 1 + \left(1 - \frac{1708}{Ra_L}\right)\left[k_1 + 2\left(\frac{Ra_L^{1/3}}{k_2}\right)^{1-\ln\left(Ra_L^{1/3}/k_2\right)}\right] + \left[\left(\frac{Ra_L}{5830}\right)^{1/3} - 1\right],$$
$$k_1 = \frac{1.44}{1 + 0.018/Pr + 0.00136/Pr^2}, \quad k_2 = 75\exp\left(1.5\,\mathrm{Pr}^{-1/2}\right) \tag{4}$$

where $Pr = \nu/\alpha$ and L is the vertical spacing between the blank underside and the furnace floor. The Nusselt numbers drop for cases as the blank equilibrates with the surroundings. The heat transfer

coefficients on the top and bottom of the blank range from 7 to 5 W/(m^{2}K) and 5.6 to 4 W/(m^{2}K), respectively, as the blank temperature varies from 100°C to 400°C.

3.2 Nominal Thermophysical Properties of Usibor® 1500 P

Accurate modeling requires careful characterization of the thermophysical and radiative properties of the furnace materials. Temperature dependent density, specific heat, and thermal conductivity for Usibor® 1500 P were supplied by ArcelorMittal [19], which are included in Table 5.

Notably, the specific heat provided by the manufacturer [19] accounts for only the sensible energy stored by ferrite and austenite during heating, but neglects the latent heat associated with the transformation of the as-received Usibor® 1500 P as it austenitizes during heating between T_{Ac1} = 720°C and T_{Ac3} = 880°C, the temperatures at which austenitization commences and is complete, respectively [20]. In a strict thermodynamics definition, the specific heat relates the change of sensible energy with temperature, but in metallurgy it is common practice to define an "effective" specific heat, $c_{p,eff}$, that accounts for simultaneous changes in sensible and latent energy during heating or cooling. Excluding this effect in a blank heating model would severely over-predict the blank heating rate and final temperature, and, if this model were used to set furnace parameters, the steel blanks may not be fully-austenitized by the end of the process.

Various measurement techniques exist for characterizing the specific heat of a material; differential scanning calorimetry (DSC), in particular, has been used to study how the 22MnB5 substrate and Al-Si layers change as Usibor® 1500 P undergoes heating [21]. The main drawback of this approach is that DSC heating rates are much slower (~1 K/s) compared to those typical of industrial heating rates (~3-5 K/s); consequently, it is not clear that the $c_{p,eff}$ inferred from differential scanning calorimetry should be directly applicable to blank furnace heating. In lieu of measured $c_{p,eff}$, Twynstra et al. [6] adopted a technique developed by Watt et al. [22] in which an effective specific heat is derived by assuming that the latent heat of austenitization is distributed uniformly between T_{Ac1} and T_{Ac3}. The change in latent heat associated with austenization of Usibor is 85 kJ/kg [11] corresponding to a specific heat step increase of 548.4 J/kg K over the phase transformation range. The original and modified specific heats are plotted in Figure 13.

Table 5: Temperature dependent properties of Usibor® 1500 P.

Temperature [°C]	Conductivity [W/(m·K)]	Density [kg/m^3]	Specific Heat [J/(kg·K)]
0	38.6	7880.8	433
50	38.9	7864.5	444
100	39.5	7848.0	465
150	39.9	7831.5	485
200	40.4	7814.8	505
250	41.0	7797.9	525
300	40.7	7781.0	547
350	40.9	7763.9	571
400	40.6	7746.6	598
450	40.1	7729.2	628
500	39.5	7711.7	662
550	38.5	7694.0	701
600	37.4	7676.2	748
650	35.9	7658.3	804
700	34.4	7640.2	876
725	37.4	7631.1	924
750	40.3	7622.0	971
800	39.7	7603.7	942
850	25.1	7585.2	825
880	26.0	7574.0	793
900	26.6	7566.6	771
950	27.3	7567.0	741
1000	27.9	7567.0	723
1050	28.3	7567.0	711
1100	28.6	7567.0	706
1150	29.2	7567.0	706
1200	29.7	7567.0	706

The results of Garcia and Deardo [15] cast some doubt on this treatment, however. They investigated the austenite formation kinetics in a 1.5% Mn steel with carbon content similar to Usibor® 1500P, and showed that the rate of phase change strongly depends on temperature; austenitization was complete within 240 seconds at 850°C, whereas it required several hours at 725°C. In a process with a relatively high heating rate, austenite formation should, therefore, take place at temperatures significantly higher than T_{Ac1}. Consequently, instead of being uniformly distributed, one may expect that the latent heat of austenitization would be concentrated closer to the T_{Ac3} temperature.

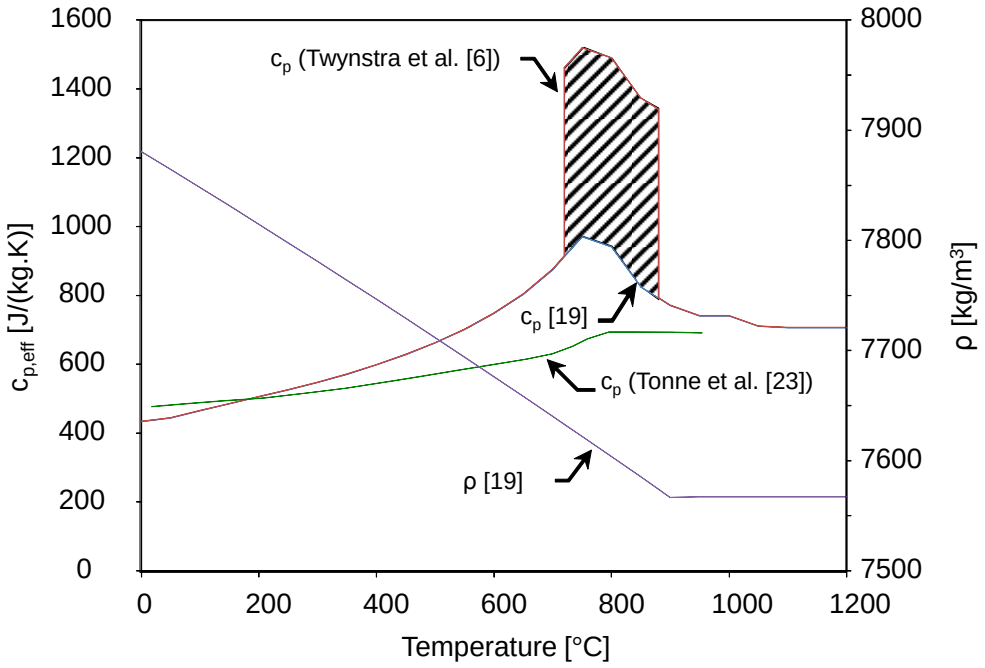

Figure 13: Twynstra et al. [6] modified the specific heat provided by the manufacturer [19] by assuming that the latent heat is distributed uniformly between T_{Ac1} and T_{Ac3}. Tonne et al. [23] inferred $c_{p,eff}$ through nonlinear regression of modeled data to thermocouple data collected in a roller hearth furnace.

In a different study, Tonne et al. [23] simultaneously inferred the specific heat and convection coefficient for Usibor® 1500 P blanks in a roller hearth furnace by regressing modeled blank temperatures to values obtained from instrumented blanks heated in the furnace. The recovered specific heat is plotted in Figure 13. While the inferred specific heat is reasonably accurate between room temperature and 300°C, it significantly under-predicts the accepted c_p for Usibor® 1500

P/22MnB5 ferritic steel provided by the manufacturer [19] at temperatures beyond 300°C. (The manufacturer-supplied specific heat for temperatures up to T_{Ac1}, corresponding to ferrite, was verified using FactSage™ [24].) This discrepancy may arise from the ill-posedness of the inference problem (i.e. the blank temperature measurements may not provide enough information to robustly estimate the convection coefficient and specific heat simultaneously), or there may be other errors in the heat transfer model used to recover these parameters; the absorptivity and emissivity of the Al-Si-Fe coating during its transformation is particularly suspect above the melting point of the Al-Si coating, ~575°C [25].

Figure 14 shows spectral emissivity data at various process temperatures, provided by the manufacturer [19]. Total absorptivities derived from the spectral emissivity curves are also shown in Figure 14 for surroundings at 500°C and 1000°C, which match values used by Tonne et al. [23] in a numerical simulation of Usibor® 1500 P blanks being heated in a roller hearth furnace. Radiative properties above 575°C should be treated with some skepticism, however, since the manufacturer provides no indication of the experimental method used to collect these data. Moreover, while the spectral emissivity is reported as a function only of blank temperature, one would expect that it should also depend on heating rate, since the Al-Si-Fe layer formation kinetics are limited by the diffusion of the species within the coating [26].

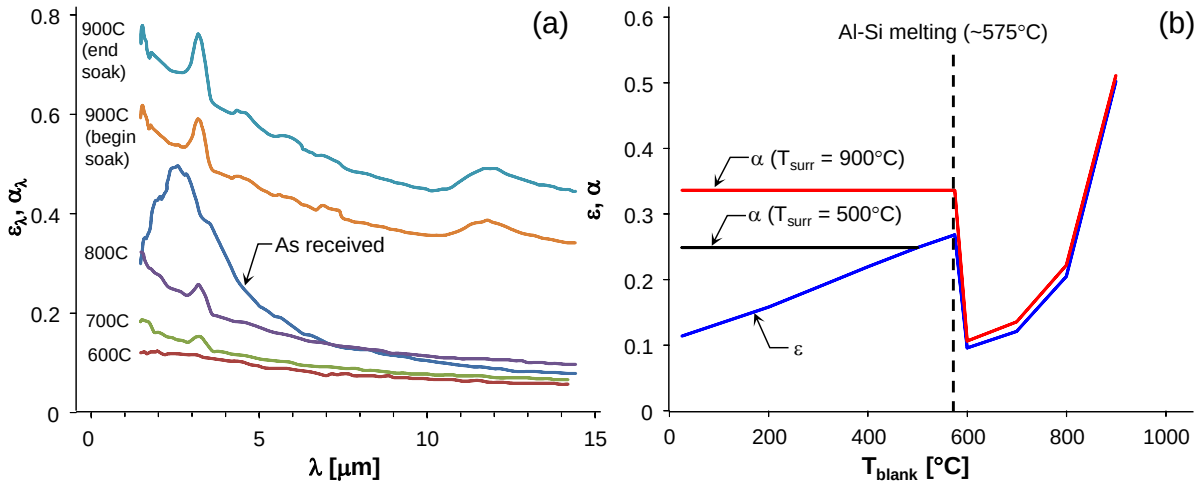

Figure 14: (a) Spectral emissivity of Usibor® 1500 P provided by the manufacturer [19]; (b) total emissivity and absorptivity calculated based on the provided spectral emissivity measurements.

3.3 Model Validation up to 500°C

Thermocouple measurements carried out on coupons heated within the muffle furnace were first used to validate the heat transfer model defined above. To this end, Eq. (1) is rearranged to isolate the specific heat,

$$c_{p,eff} = \frac{2\alpha\sigma T_{surr}^4 - 2\varepsilon\sigma T_s^4 + \left(h_{top} + h_{bottom}\right)\left(T_{surr} - T_s\right)}{\rho w \, dT_s/dt} \tag{5}$$

Since both the specific heat and the spectral emissivity of Usibor® 1500 P are known to a high degree of certainty below 575°C, the first series of tests were carried out with the furnace set to 500°C, and the model accuracy was assessed by comparing the c_p inferred from Eq. (5) to the manufacturer's value.

A finite difference approximation of the coupon heating rate results in an unacceptably-noisy approximation of dT_s/dt. Instead, this value was found by deconvolving a Volterra integral equation of the first kind (IFK)

$$T_s(t) - T_0 = \int_0^t \left.\frac{dT_s}{dt}\right|_{t^*} dt^* \tag{6}$$

Equation (6) is discretized into a matrix equation, $\mathbf{Ax} = \mathbf{b}$, where $\mathbf{A}$ is a lower triangular matrix, $\mathbf{x}$ contains dT_s/dt at various process times, and $b_i = T_s(t_i) - T_0$. Volterra IFKs are mathematically ill-posed, and consequently $\mathbf{A}$ is ill-conditioned; this means that measurement noise contaminating $\mathbf{b}$ is amplified into large variations in $\mathbf{x}$. A first-order Tikhonov regularization [27] [28] is used to stabilize this inversion by solving the least-squares problem

$$\mathbf{x}_\lambda = \arg\min \left\| \begin{bmatrix} \mathbf{A} \\ \lambda\mathbf{L} \end{bmatrix} x - \begin{bmatrix} \mathbf{b} \\ \mathbf{0} \end{bmatrix} \right\|_2^2 \tag{7}$$

where $\mathbf{L}$ is a smoothing matrix that approximates the first-derivative and the regularization parameter, λ, was chosen using the L-curve curvature technique [28]. This procedure is shown schematically in Figure 15.

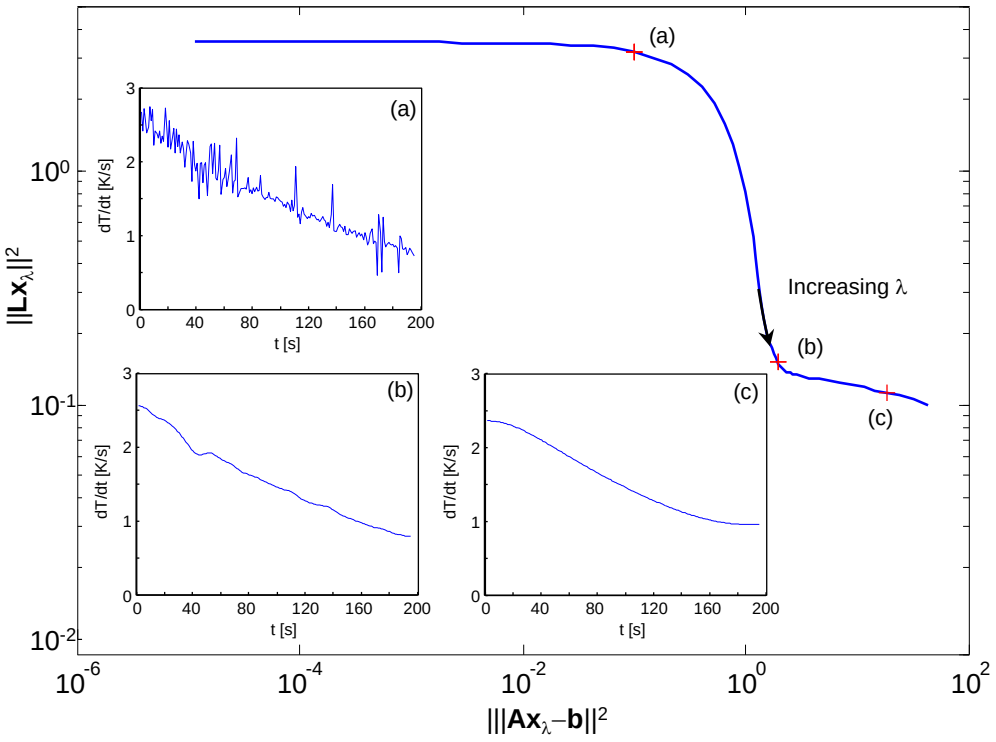

Figure 15: Schematic of first-order Tikhonov regularization using the L-curve. Plots (a), (b), and (c) show temperature heating rates obtained using insufficient, optimal, and excessive regularization.

The surroundings temperature, T_{surr}, is also needed to calculate the irradiation of coupon by the furnace surroundings. The simplest choice for this parameter is the final steady state coupon temperature, $T_{s,ss}$, which implicitly assumes that: (i) the coupon has reached radiative equilibrium with the surroundings; and (ii) the surroundings remain isothermal throughout the heating process. The first assumption is reasonable as long as the coupon temperature plateaus at the end of the process, as do the heating profiles in Figure 10. The second assumption is somewhat more problematic, since it does not account for furnace hot and cold spots and process variations as the heaters cycle on and off and when the furnace door is opened and closed. To investigate the validity of these assumptions, we monitored the furnace wall temperature using K-type thermocouples, as mentioned in Chapter 2. Figure 11 shows that the surrounding temperatures vary both in location and throughout the blank heating process.

Accordingly, we account for the temporal and spatial variation in surrounding temperature through a detailed model of the radiation exchange between the blank and the furnace walls using

exchange factors [29]. In this approach the furnace walls are discretized into rectangular sub-surfaces that are approximated as isothermal, and an "effective" surrounding temperature, $T_{surr,eff}$, can be found by rearranging

$$Q_{rad} = A_s \sigma \left[T_{surr,eff}^4 (t) - T_s^4 (t) \right] = \sum_{i=1}^{n} \varepsilon_i \mathcal{F}_{i-s} A_i \sigma \left[T_i^4 (t) - T_s^4 (t) \right] \tag{8}$$

where A_s is the total (top and bottom) surface area of the coupon, ε_i and A_i are the total emissivity and area of the *ith* sub-surface, and $\mathcal{F}_{i-s}$ is the exchange factor between the *ith* sub-surface and the top and bottom surfaces of the coupon. The exchange factor is found by a Monte Carlo technique [29]. In this study, the emissivity of the refractory insulation of the furnace walls is taken to be 0.8, based on the value used by Twynstra et al. [6].

A sensitivity analysis shows that uncertainty in the surrounding temperature, T_{surr}, dominates uncertainty in the inferred specific heat. Accordingly, uncertainty in c_p is estimated by

$$\Delta c_p = \frac{\partial c_p}{\partial T_{surr}} \Delta T_{surr} = \frac{8 \alpha T_{surr}^3 + \left(h_{top} + h_{bottom} \right)}{\rho w \, dT_s / dt} \Delta T_{surr} \tag{9}$$

where ΔT_{surr} is taken to be ± 25K based on the variation seen in Figure 11.

The specific heats inferred using Eq. (5) are plotted in Figure 16. The dashed lines correspond to specific heats inferred from individual tests, which indicate a high degree of repeatability between tests. (Tests carried out on thinner coupons, not shown here, resulted in larger variability in the inferred c_p.) Both techniques for calculating T_{surr} provide c_p values that are consistent with the value provided by the manufacturer within the expected uncertainty, which increases as the coupons thermally-equilibrate with the furnace surroundings and dT_s/dt tends to zero.

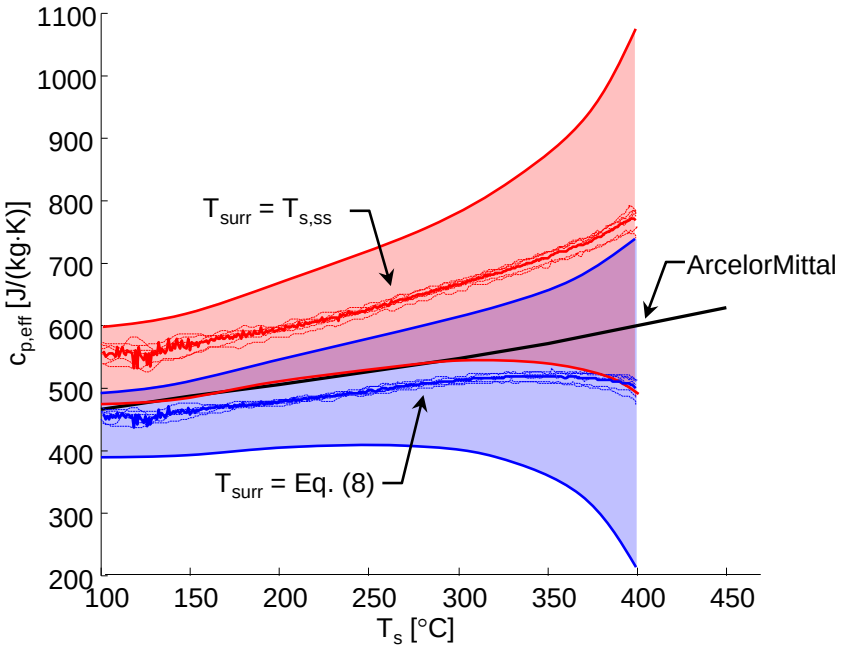

Figure 16: Specific heat of Usibor® 1500 P inferred from low temperature muffle furnace experiments. Dashed curves indicate individual measurements, solid curves indicate averages, and shaded regions indicate uncertainty associated with T_{surr}.

3.4 Characterization of Thermophysical Properties of Usibor® 1500 P

3.4.1 Latent Heat of Austenitization

We next extend the muffle furnace experiments to characterize the effective specific heat of 22MnB5 during austenitization. A major complicating factor is that the radiative properties of Usibor® 1500 P change beyond the melting point of the Al-Si coating, which will influence the inferred $c_{p,eff}$. To avoid this uncertainty, the Al-Si coating is removed from the Usibor® 1500 P coupons using a sodium hydroxide solution, and the stripped 22MnB5 coupons are coated with a boron nitride (BN) aerosol spray to prevent the coupons from oxidizing and decarborizing within the furnace. The spectral emissivity of the BN-coated coupons is then characterized using an SOC 400T FTIR reflectometer, and these values are used to derive the total emissivity at various blank temperatures as shown in Figure 17. Unlike the Al-Si coating, which undergoes a physical and chemical transformation during heating, BN is resilient at the temperatures typical of furnaces used in HFDQ; a comparison of

spectral emissivity data measured on unheated and post-heated BN-coated 22MnB5 blanks revealed no change in ε_λ.

The specific heats inferred from this procedure are plotted in Figure 18. In this case the value obtained with both $T_{surr} = T_{blank,ss}$ and the detailed radiative model are very similar, and both slightly overestimate the accepted value of c_p before T_{Ac1}. This result can be considered further validation of the muffle furnace heat transfer model, since it predicts the specific heat for 22MnB5 with reasonable accuracy below T_{Ac1} for both Usibor® 1500P and the BN-coated 22MnB5, even though the radiative properties of these surfaces are significantly different.

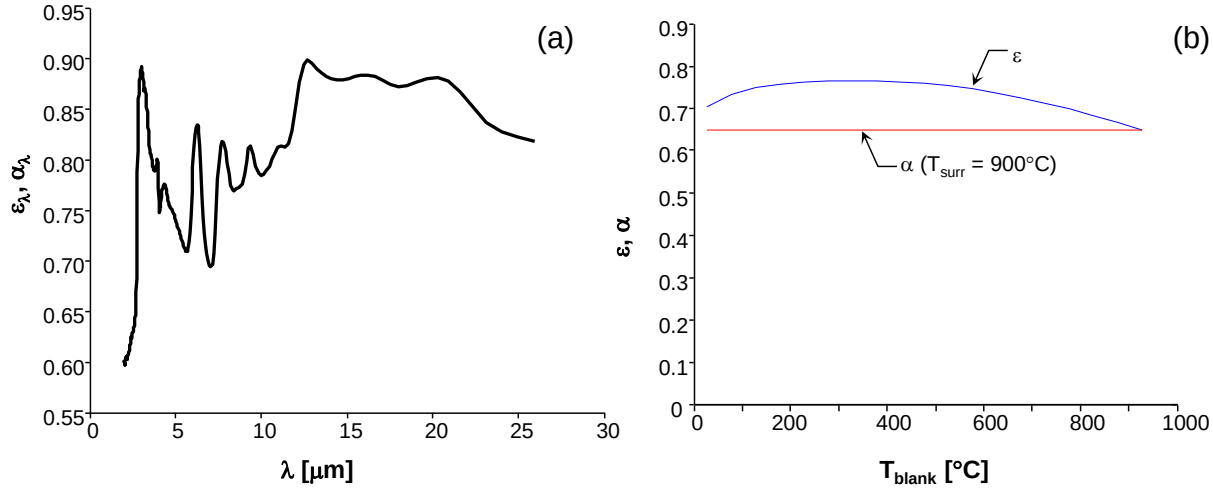

Figure 17: (a) Spectral emissivity of BN-coated 22MnB5; (b) total emissivity and absorptivity.

Unlike the results of Tonne et al. [23], however, the specific heat inferred from the blank temperature increases abruptly beyond T_{Ac1}, corresponding to the onset of austenitization. These curves also show that, in contrast to the uniformly-distributed latent heat of austenitization assumed by Watt et al. [22] and Twynstra et al. [6], $c_{p,eff}$ is not uniformly-distributed between T_{Ac1} and T_{Ac3}. Rather, the peak effective specific heat is slightly higher at T_{Ac1} and drops abruptly as the blank temperature approaches T_{Ac3}. (This also contradicts our hypothesis that $c_{p,eff}$ would be larger at temperatures closer to T_{Ac3} due to the greater rate of austenitization at higher temperature.) Specific heats inferred close to T_{Ac3} become unreliable, however, since the denominator of Eq. (5) approaches zero as the coupon equilibrates with the furnace surroundings.

The effective specific heat between T_{Ac1} and T_{Ac3} is further investigated by heating a 2.4 mm thick Usibor® 1500P coupon in a Gleeble® 3500 thermomechanical simulator. The Gleeble heats the sample according to a programmed heating curve using Joule heating; the electric current supplied to

the sample is regulated using a PID controller with input from a thermocouple welded to the coupon. While the power angle has not been calibrated (and also does not account for heat transfer losses from the coupon) variation in the time-dependent power angle indicates the changing effective specific heat as the coupon is heated. Accordingly, we programmed the Gleeble with thermocouple data obtained from the muffle furnace data shown in Figure 10 and recorded the power angle as the coupon was heated. Figure 19 shows that the power angle is similar in trend to the specific heat provided by the manufacturer, although the Gleeble power angle increases at a somewhat greater rate with respect to temperature approaching T_{Ac1}; this would be expected, since the heat transfer losses from the Usibor® 1500P coupon (particularly radiation losses to the Gleeble measurement chamber) increase with increasing temperature. Both the Gleeble power angle and the inferred $c_{p,eff}$ increase abruptly at T_{Ac1}, which again suggests that most austenitization occurs closer to T_{Ac1}. The power angle appears to present a more plausible $c_{p,eff}$ profile at temperatures closer to T_{Ac3} compared to the value inferred from the muffle furnace measurements.

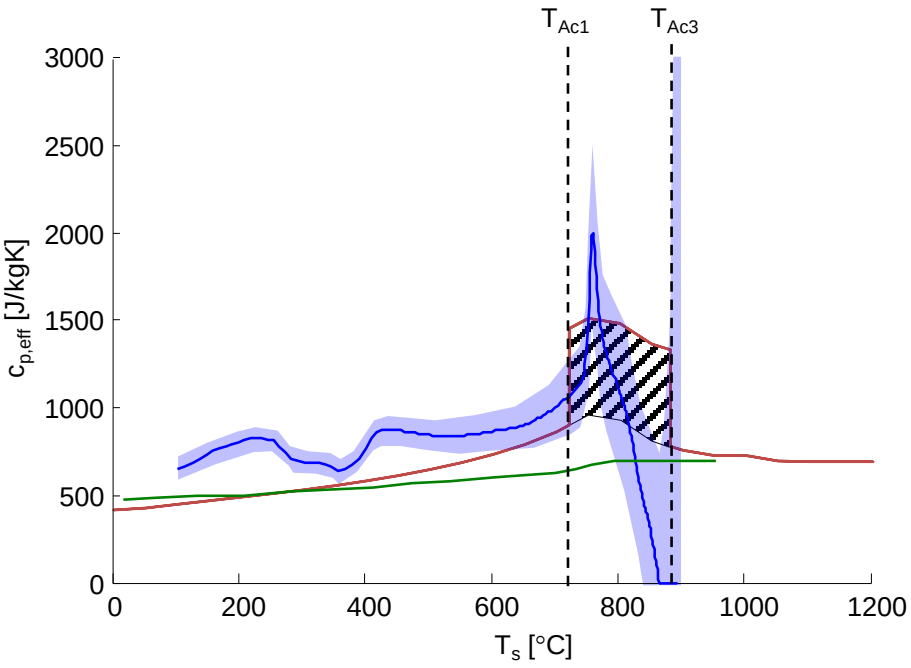

Figure 18: Effective specific heats for 22MnB5 at high temperatures. Present values are obtained from temperature measurements on BN-coated 22MnB5 blanks within the muffle furnace, using Eq. (8) to find T_{surr}. The shaded region indicates uncertainty in c_p due to uncertainty in T_{surr}. Other curves are as labeled in Figure 13.

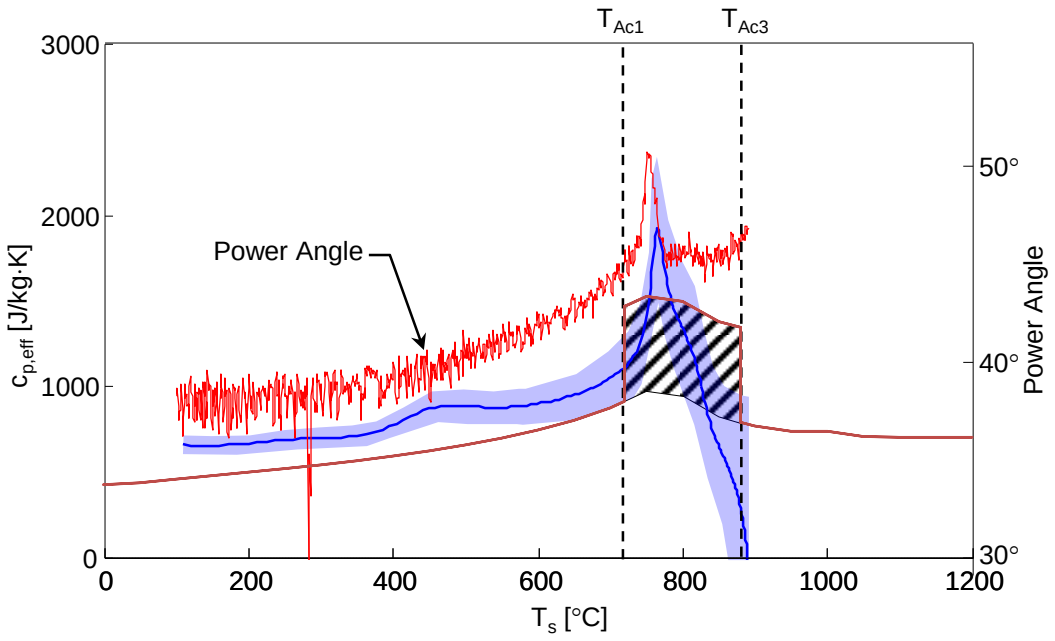

Figure 19: Comparison of Gleeble power angle with $c_{p,eff}$ inferred from muffle furnace measurements.

Based on these observations, a new $c_{p,eff}$ for modeling Usibor® 1500 P austenitization is derived following Watt et al. [22] and Twynstra et al. [6], where the manufacturer-specified specific heat, whch considers only sensible energy, is modified by distributing the latent heat of austenitization (85 kJ/kg [30]), between T_{Ac1} and T_{Ac3}; in this work, however, the latent heat of austenitization follows a triangular profile skewed towards T_{Ac1}, as shown in Figure 20.

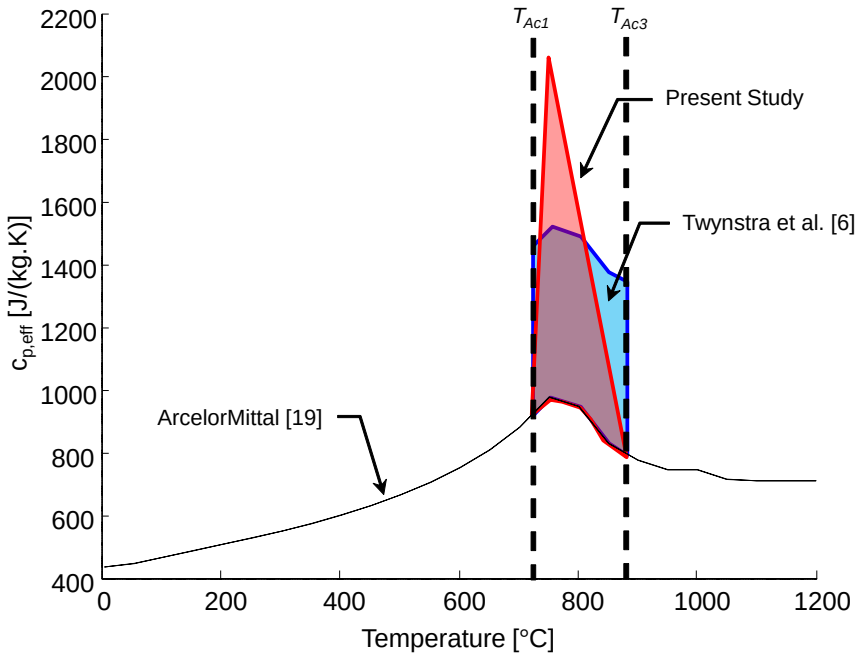

Figure 20: Modeled $c_{p,eff}$ assuming that the latent heat of austenitization is absorbed according to a triangular profile between T_{Ac1} and T_{Ac3}. The shaded areas correspond to the latent heat of austenitization of 22MnB5, 85 kJ/kg [30].

3.4.2 Characterization of Radiative Properties of Usibor® 1500 P

Accurate knowledge of the radiative properties of the Usibor® 1500 P blanks is essential to modeling blank temperature as radiation is the dominant mode of heat transfer within the furnace. The physical and chemical transformation of the Al-Si layer as it melts at 575°C alters the radiative properties of the blanks, consequently, changing the heat transfer to the blank.

The characterization of radiative properties was carried out using OceanOptics NIRQuest near infrared spectrometer and a SOC 400 FTIR reflectometer as presented by Chester et al. [26]. The spectrometer is capable of measuring *in-situ* spectral emissivity of a coupon heated in the Gleeble; however it is only effective in a narrow range of wavelength from 0.9 to 2.5 μm which is insufficient to calculate total emissivity at the temperatures involved in this study. Thus, FTIR reflectometer was used in addition to the NIR spectrometer to obtain spectral emissivity over the required wavelength range. The FTIR reflectometer measures spectral reflectance of a coupon between the wavelengths of 2 to 25 μm; however it is significantly slower than NIR spectrometer and is therefore is not well-suited to perform *in-situ* measurements at higher temperatures. Thus steel coupons were heated in the

Gleeble according to a temperature history obtained from roller hearth furnace tests and quenched in air to preserve the chemical and physical state of the coating. The air quenched coupons were later analyzed using the FTIR reflectometer. The spectral emissivity measurements were carried out on samples quenched at 700, 800, 900, and 935°C as shown in Figure 21.

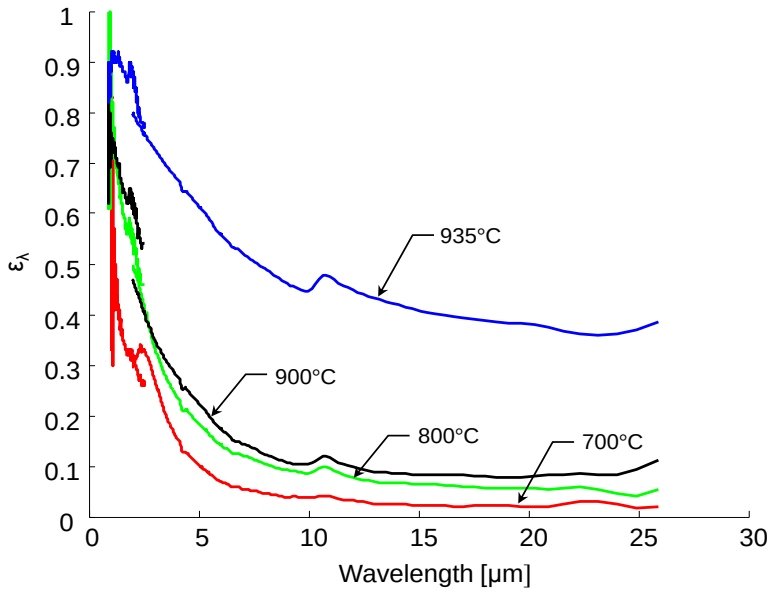

Figure 21: Spectral emissivity measurements carried out using NIR spectrometer (0.9 to 2.5μm) and FTIR reflectometer (2 to 25 μm).

However, the FTIR is not suitable to measure the spectral emissivity of coupons near the melting temperature of Al-Si layer. Air quenching resulted in distortions in the blank surface between 575 - 700°C due to the air flow over molten Al-Si layer. Thus, the FTIR reflectometer could not be used for this temperature range, and the total emissivity was estimated based solely on the measurements carried out using the NIR spectrometer on coupons heated in the Gleeble. The spectral emissivity measurements made with a NIR spectrometer on Gleeble-heated Usibor® 1500 P coupons show that, upon melting, ε_λ drops to a value of 0.2 between 900 and 2500 nm [26]. In the absence of further information, it was assumed that this value extends into the mid-infrared to give a total absorptivity of 0.2 instead of 0.1 at 575°C. Figure 22 shows the updated ε and α compared to the values provided by the manufacturer. Data are linearly interpolated between the temperatures at which the experiments were performed. Linear interpolation is reasonable in this case as there are no sudden changes to the radiative properties preceding the melting of Al-Si layer. The measured ε and

α are generally higher than the values provided by the manufacturer preceding melting of Al-Si layer. Upon the melting of the Al-Si layer, α drops to 0.2 from 0.33 and little change is observed till 700 °C. However, after 700°C both α and ε increase as iron from the substrate steel diffuses further into the Al-Si layer and finally reach a maximum value of 0.66 at 935°C.

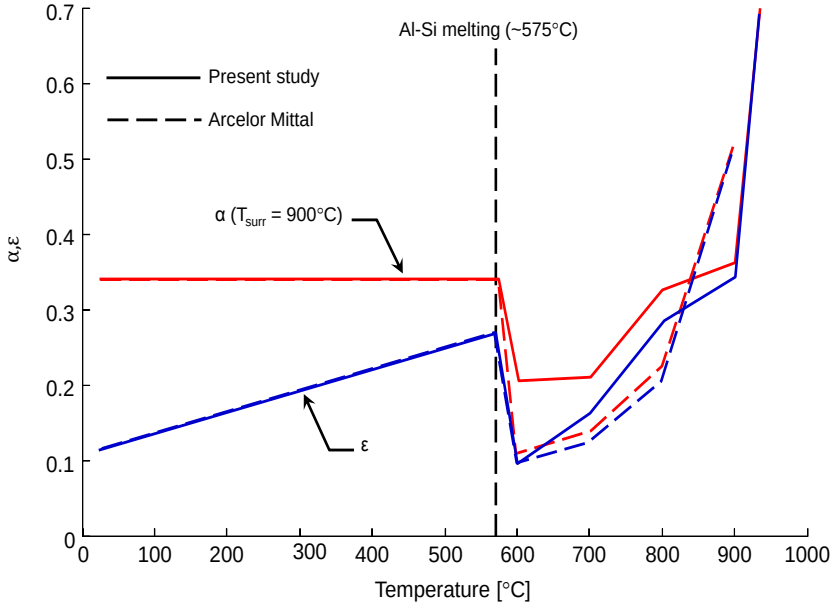

Figure 22: Total emissivity and total absorptivity based on the new measurements.

Validation of the radiative properties obtained in the present study is carried out by comparing the inferred effective specific heat of Usibor® 1500 P calculated using Eq. (5) and the temperature history of unpatched blank shown in Figure 10. The difference in the inferred $c_{p,eff}$ due to the changes in the radiative properties is highlighted in Figure 23. The inferred specific heat obtained using the radiative properties supplied by the manufacturer, matches the accepted value at lower temperatures, but abruptly drops at 575°C, which corresponds with the Al-Si melting point. This result indicates that the absorptivity of the molten Al-Si coating is higher than the value of 0.10 reported by the manufacturer. As expected, a smaller drop in inferred $c_{p,eff}$ is observed at the melting point of Al-Si layer when α is assumed to be 0.20 instead of 0.10. Moreover, inferred $c_{p,eff}$ calculated using the updated radiative properties is consistent with the findings of Section 3.4.1 between T_{Ac1} and T_{Ac3} temperature; a non-uniform distribution of latent heat of austenitization with a peak at 765°C is similar to the one presented in Figure 20.

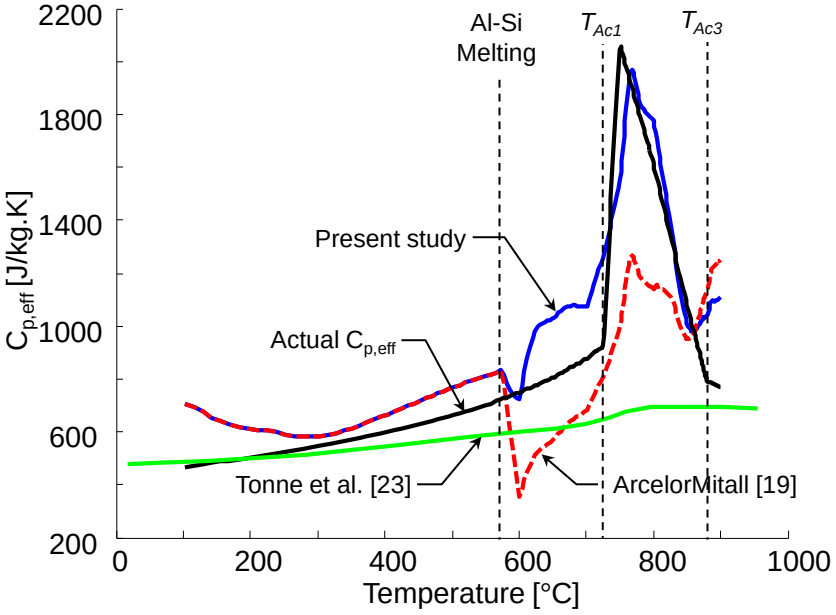

Figure 23: Inferred effective specific heat calculated using Eq. (5) and radiative properties presented in Figure 14 and Figure 22.

Chapter 4
Heat Transfer Model of Patched Blanks

The heat transfer model of the muffle furnace presented in Chapter 3 was used mainly to validate the characterization of thermophysical properties of Usibor® 1500 P. A more elaborate version of this model is presented in this chapter that can be used to predict the transient temperature of patched blanks heated in the muffle furnace and the roller hearth furnace. This chapter is concluded by evaluating the effectiveness of high absorbtant coatings to minimize non-uniform heating observed within patched blanks.

4.1 Blank Discretization

The temperature measurements presented in Chapter 2 of patched blanks show that there is a significant variation in the heating rate of patched blanks. This is largely due to the additional thermal mass of the patch and due to the reduced conduction heat transfer between the patch and substrate blank. The spot-welded patch is not in perfect contact with the substrate blank, which reduces heat transfer between the patch and substrate blank. Accordingly, blanks are discretized into small rectangular volume elements of 10 mm × 10 mm × thickness such that the temperature variation throughout the blank can be represented by the heat transfer model. The blanks heated in the muffle furnace can be easily discretized due to their rectangular shape; however, the geometry of B-pillar and hinge pillar blanks is simplified prior to discretization as shown in Figure 24.

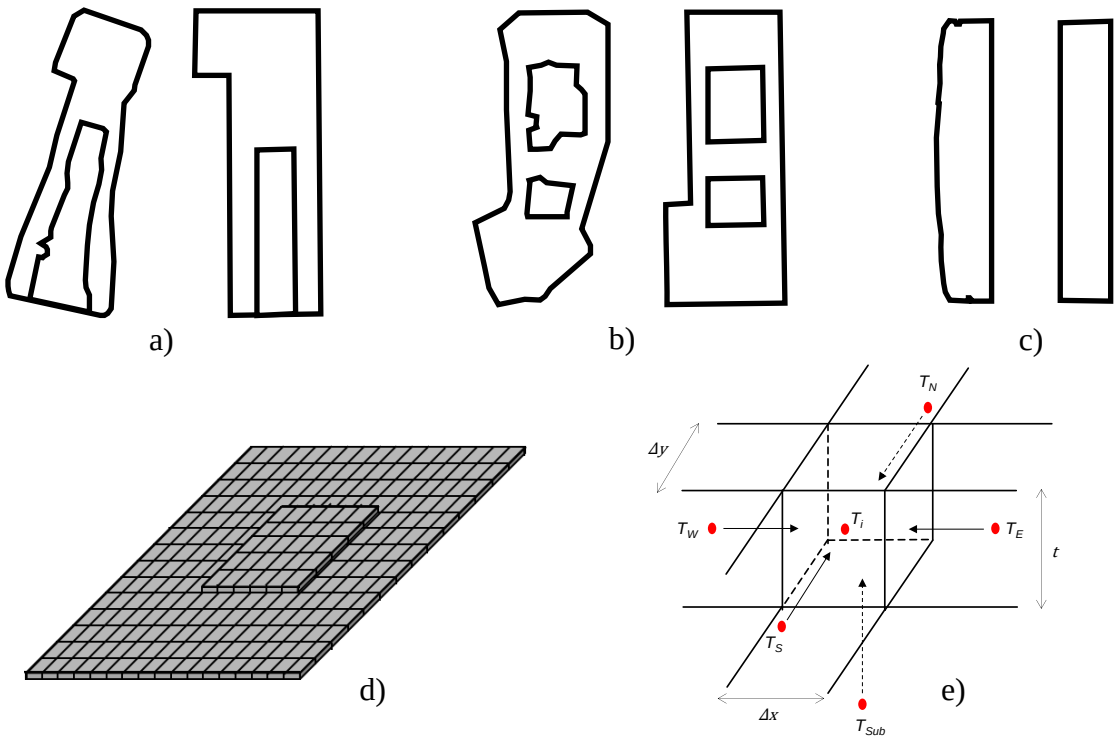

Figure 24: Geometry simplifications of a) B-pillar, b) hinge pillar, and c) bumper blanks. Discretized geometry along with conduction to an internal volume element is shown in d) and e) respectively.

4.2 Governing Equations

In both the roller hearth furnace and the muffle furnace, heat is transferred to the blank via radiation and convection, and heat conduction from the platform and rollers is assumed to be negligible. Thus, total net heat input to each volume element is the summation of heat received through radiation and convection at the exposed surface areas and through conduction from its adjacent volume elements. Consequently, the temperature of the *ith* volume element is governed by

$$\rho_i c_{p,eff,i} V_i \frac{dT_i}{dt} = \dot{Q}_{net,\mathrm{rad},i} + \dot{Q}_{net,\mathrm{conv},i} + \dot{Q}_{net,cond,i} = \dot{Q}_{net,i} \tag{10}$$

where ρ_i, $c_{p,eff,i}$ and V_i are the density, effective specific heat and the volume of the *ith* volume element. Net radiation, $Q_{net,rad,i}$, to the blank can be expressed by

$$\dot{Q}_{net,rad,i} = A_i \alpha_i \sigma T_{surr}^4 - A_i \varepsilon_i \sigma T_i^4(t) \tag{11}$$

which assumes that the blank is irradiated equally from above and below by large and isothermal furnace surroundings. This assumption is justified based on the temperature measurements obtained during furnace characterization. The surrounding temperature, $T_{surr,}$ is assumed to be equal to the furnace set-point temperature for both the furnaces and it remains approximately constant throughout the heating for the muffle furnace. However, in the roller hearth furnace, zone temperature varies throughout the furnace, therefore, T_{surr} changes as the blank is conveyed through the furnace. The local furnace air and surrounding surface temperatures are assumed to be equal, and are estimated by linear interpolation between the TC sensor locations within each zone.

Net convection to each volume element is estimated using

$$\dot{Q}_{net,\mathrm{conv},i} = A_{i,top} h_{top} \left(T_\infty - T_i\right) + A_{i,bottom} h_{bottom} \left(T_\infty - T_i\right) \tag{12}$$

and local air temperature, T_∞, is assumed to be equal to the surrounding surface temperatures. The convection coefficients, h_{top} and h_{bottom}, are calculated using Eq. (2) and Eq. (4), respectively, for the blanks heated in muffle furnace, however, Eq. (4) is only valid for cavities and cannot be applied to the blanks heated in roller hearth furnace. Due to the slow blank speed and the small gap between the baffles and the blank surface, the furnace atmosphere in roller hearth furnace can be approximated as quiescent, so the convection coefficients were derived using Eq. (2) and Eq. (13) adjusted for larger blanks [31]. The Nusselt numbers given by the presented correlations are highest at the start of the heating process and eventually reach zero as the blank equilibrates with its surroundings. Hence, the convection coefficients, h_{top} and h_{bottom}, range from 7 to 0 W/(m^{2}K) and 5.6 to 0 W/(m^{2}K), respectively, for the muffle furnace as the blank temperature varies from 25 to 930°C. In the roller hearth furnace however, h_{top} and h_{bottom} range from 4 to 0 W/(m^{2}K) and 9 to 0 W/(m^{2}K), respectively, throughout the heating process.

$$Nu_{L,\mathrm{bottom}} = \frac{h_{bottom} L}{k_{air}} = 0.54 Ra_L^{1/4} \tag{13}$$

Conduction within the unpatched blanks was modeled as two-dimensional and three-dimensional for the patched blanks. Adiabatic boundary conditions were applied to outermost blank edges. For an element within the interior of a blank, the net heat conduction is given by

$$\dot{Q}_{net,cond,i} = kt\left[\Delta x \frac{T_N - T_i}{\Delta y} + \Delta x \frac{T_S - T_i}{\Delta y} + \Delta y \frac{T_E - T_i}{\Delta x} + \Delta y \frac{T_W - T_i}{\Delta x}\right] + U \Delta x \Delta y \left(T_{sub} - T_i\right) \tag{14}$$

where

$$U = \frac{k_{air}}{t_{gap}} \tag{15}$$

corresponding to the element arrangement shown in Figure 24 (e), where k and k_{air} are the thermal conductivities of blank and air, respectively, and t and t_{gap} are the blank thickness and air gap thickness between substrate and patch blank, respectively. An overall heat transfer coefficient between substrate and patch blank, U, is given by Eq. (15) which ranges from 260 to 760 W/m^{2}K for air temperatures between 25 to 900°C if the air gap thickness is assumed to be 0.1mm.

The transient temperature of the volume elements is then solved by numerically integrating Eq. (10) using an explicit Euler scheme,

$$T_i^{k+1} = T_i^k + \frac{\dot{Q}_{net,i}}{\rho_i V_i c_{p,i}} \Delta t \tag{16}$$

where a time step of Δt = 0.25 seconds was found to provide an acceptable balance between time resolution and computation time for the model. At each time step, the net heat transferred to each volume element via radiation, convection and conduction heat transfer is calculated using the procedure described above and the resulting change in the temperature due to this heat transfer is calculated using Eq. (16).

4.3 Model Validation

The accuracy of the model presented in the previous section is assessed by comparing the modeled and measured temperature of unpatched and patched blanks with various thicknesses.

4.3.1 Muffle Furnace

The modeled and measured temperature of blanks heated in the muffle furnace with unpatched and patched thickness of 1.3 and 2.6 mm, respectively, is shown in Figure 25 (a). The modeled temperature of the unpatched section matches the measured temperature over the complete range; however, the modeled temperature of a patch is significantly under-predicted above 750°C. Further insight into heat transfer during blank heating is obtained by analyzing the changes in heating rate of modeled and measured temperature. Figure 25 (b) shows two abrupt drops in the heating rate of both the patched and the unpatched sections of the blank. The first drop in heating rate occurs at 575°C due to a decrease in absorptivity of the blank as the Al-Si coating starts melting; a second drop occurs at 720°C as the ferrite starts to transform into austenite. The experimental data also shows an increase in heating rate at 850°C that is not replicated in the model, which may suggest that the majority of the

ferrite is transformed into austenite by 850°C. Thus, the $c_{p,eff}$ plotted in Figure 20 might over-predict the austenitization occurring at higher temperatures.

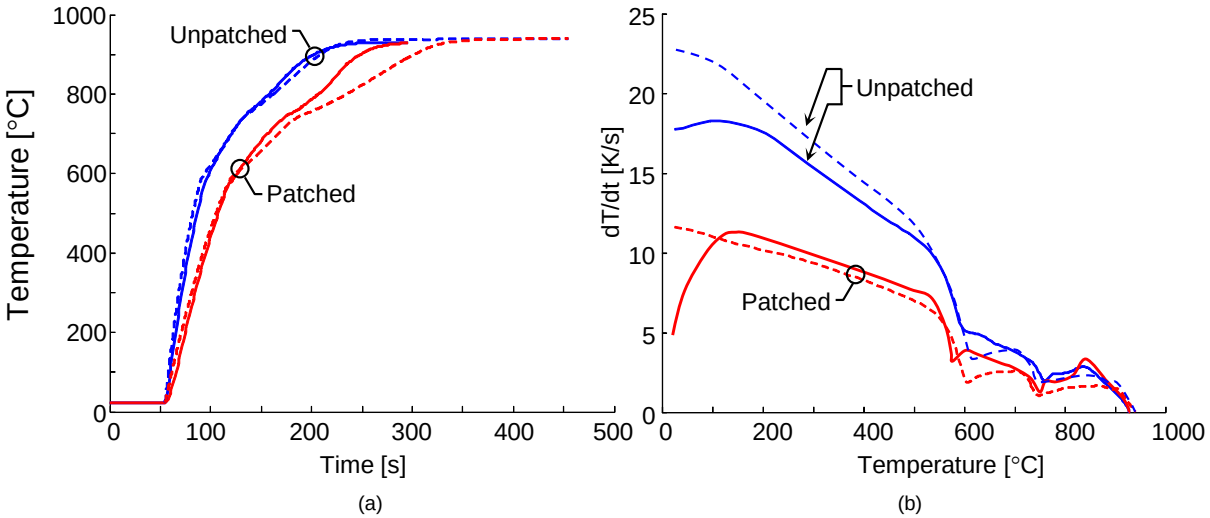

Figure 25: Comparison of modeled and measured (a) temperature histories (b) heating rates for patched blanks heated within the muffle furnace. (Solid and dashed lines denote measurements and modeled results, respectively.)

4.3.2 Roller Hearth Furnace

Figure 26 shows the comparison between modeled and measured temperature and heating rate of the bumper, hinge and b-pillar blanks heated in roller hearth furnace. The hinge and b-pillar blanks are patched and have effective thicknesses of 2.6 and 3.0mm, respectively, whereas the thickness of unpatched bumper blank is 1.3mm. As shown in Figure 26 (a), the modeled temperature of bumper blank is within 5% of measured values, with the largest difference of 28°C occurring at 850°C. However, a larger difference is observed in hinge and B-pillar blanks. At 930°C, the modeled temperature is 30°C and 50°C lower than the measured value for the hinge and B-pillar blanks, respectively. For all three blanks, the model temperature is consistently lower than the measured temperature during phase transformation of ferrite into austenite. Some insight into this discrepancy is provided by observing the heating rate of measured and modeled temperatures as shown in Figure 26 (b). The modeled temperature increases approximately linearly after the melting of the Al-Si layer until the blank reaches equilibrium with its surroundings, however, a significant increase in the heating rate is observed in the measured temperature of the B-pillar and hinge pillar between 820 to 860°C. Consequently, the model predicts longer heating times to reach

900°C as it fails to replicate the increased heating rate at the end of the heating. As shown in Table 6, model predicts 14, 21 and 44 seconds longer heating time to reach 900°C for the bumper, hinge and B-pillar blanks, respectively.

Table 6: Required heating time to reach 900°C for blanks heated in roller heart furnace.

	Heating Time [s]		
	Measured	Model	Δt
Bumper	188	202	14
Hinge pillar	296	317	21
B-pillar	321	365	44

One possible explanation for this discrepancy is that the distribution of latent heat used in the model over-estimates the amount of austenitization occurring near the T_{Ac3} temperature for the hinge and B-pillar blanks. It takes approximately 110 seconds for the hinge and B-pillar blanks to be heated from T_{Ac1} to T_{Ac3} temperature, whereas it only takes 75 seconds for the bumper blanks. The longer soak time of thicker blanks during transformation might result in most of the ferrite being transformed into austenite by 820°C; thus latent heat of austenitization would essentially be zero beyond this temperature. There is also some uncertainty in the modeled temperature due to the variation in the surrounding temperature of the roller hearth furnace. In addition, the assumptions built into the heat transfer model also result in some uncertainty in the modeled temperature. Complete sensitivity analysis of the modeled temperature is presented in the appendix.

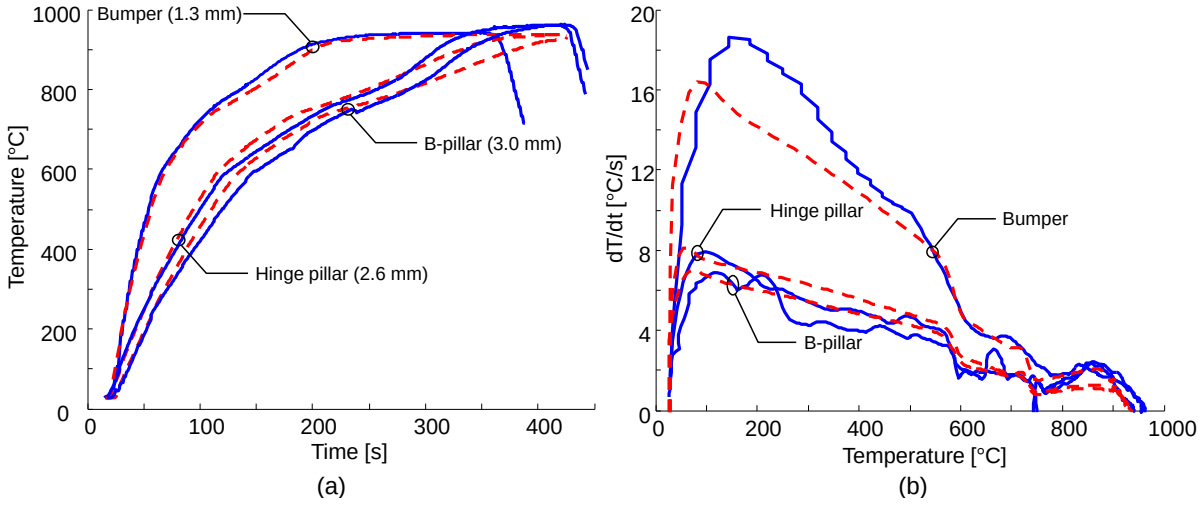

Figure 26: Comparison of modeled and measured (a) temperature histories (b) heating rates for patched blanks heated within the roller hearth furnace. (Solid and dashed lines denote measurements and modeled results, respectively.)

4.4 Uniform Patch Heating Through Tailored Radiative Properties

Since blank heating is mostly radiative, small changes in the blank absorptivity would significantly increase the blank heating rate. Therefore, changing the radiative properties presents a possible technique for controlling the blank heating rate. This approach has been employed by Wilsius et al. [32], who used highly-reflective "masks" on single-gage blanks to achieve tailoring during furnace heating through incomplete austenitization.

In this study we investigate the possibility of achieving uniform blank heating by painting the exposed patch surface with a highly-absorbing boron nitride (BN) aerosol coating. Boron nitride is chemically inert and robust to high temperatures; spectral reflectivity measurements made on BN-coated 22MnB5 blanks pre- and post-furnace heating confirmed a negligible change in spectral emissivity, and Figure 17 shows that the total absorptivity of the BN coating is roughly twice that of the as-received Al-Si coated 22MnB5 steel, making it seemingly ideal to compensate for the doubled thickness of the patched regions. This was confirmed by adjusting the properties used in the heat transfer model of the muffle furnace. Figure 27 (a) shows that the modeled patch and unpatched temperatures are nearly identical until approximately 800°C, at which point the heating rate of the patched area drops relative to the unpatched area.

Further measurements were carried out in the muffle furnace with the outside of the patch painted with boron nitride using the apparatus shown in Figure 9. Figure 27 (b) shows that, in contrast to the modeled results, the temperatures of the patched and unpatched regions are nearly identical throughout the heating process. The BN-coated patches achieved complete austenitization approximately 60 seconds earlier compared to the uncoated patches.

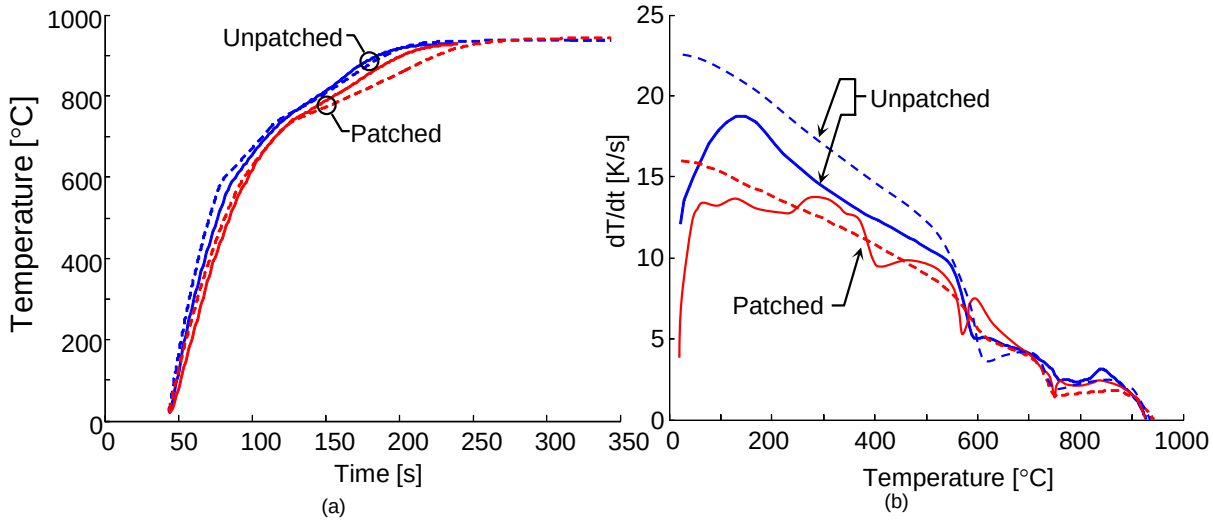

Figure 27: (a) Modeled and measured temperatures for patched blanks with a boron nitride coating on the patch heated within muffle furnace (b) heating rates of modeled and measured temperature with boron nitride coated patch. (Solid and dashed lines denote measurements and modeled results, respectively.)

Similarly, the heat transfer model of the roller hearth furnace was adjusted to determine the impact of boron nitride coating on blank heating. Figure 28 shows the modeled blank temperature of the unpatched and the patched regions of the blank; it shows that the required heating time to reach complete austenitization would decrease by approximately 50 seconds if the boron coating is applied to the patch. These results were further validated by performing boron nitride coated blank trials in the roller hearth furnace at Formet Industries. During heating, the blank temperature was measured at two locations; a thermocouple was attached to the substrate blank directly below the painted patch and another thermocouple was attached to the unpatched region far from the patch. Figure 28 shows the results obtained from these blanks trials along with the modeled blank temperature. While the non-uniform heating within the blank is not completely eliminated, there is a noticeable decrease in the required heating time. Blanks coated with Al-Si and BN coating reached 900°C in 325 and 225

seconds, respectively; thus showing that the patched blanks can be heated more uniformly and in less time by applying a BN coating to the surface of the patch.

Differences observed in the results of muffle and roller hearth furnaces are mainly due to the location at which the temperature was measured during experiments. In the roller hearth furnace, blanks are conveyed through the furnace with the patch facing downward (quenching dies are designed to accept blanks this way), therefore, there is no direct way of measuring the temperature of the patch itself. Instead the temperature of the substrate blank directly above the patch was measured whereas, in the muffle furnace, the temperature of the patch itself was measured. The boron nitride coated patch reaches higher temperature than the substrate blank underneath it as the conduction between the patch and substrate blank is hindered by an air gap, as highlighted by the measured temperatures shown in Figure 27 and Figure 28.

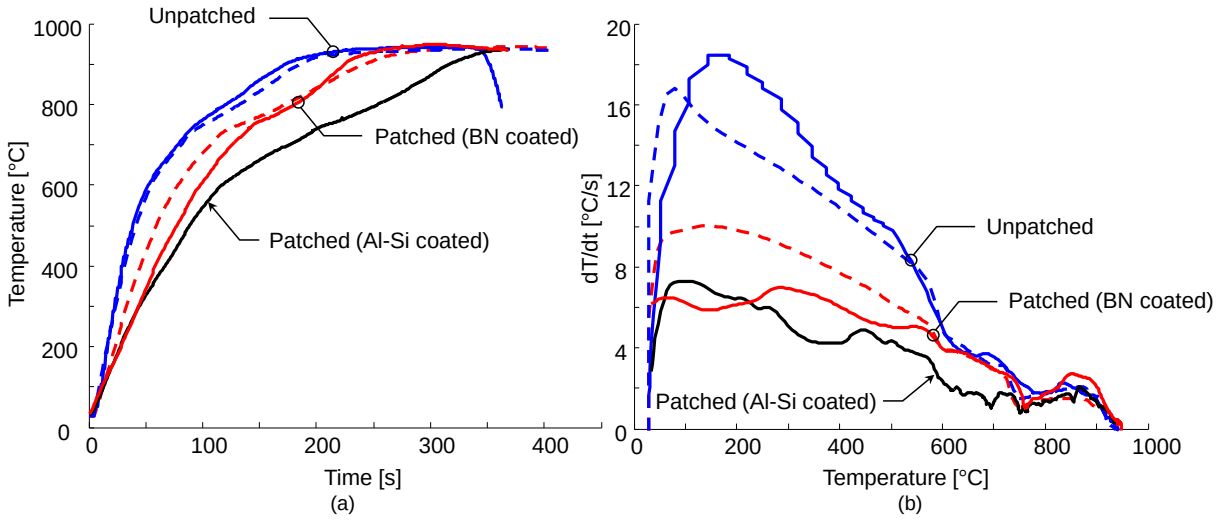

Figure 28: (a) Modeled and measured temperatures for patched blanks with a boron nitride coating on the patch heated within roller hearth furnace (b) heating rates of modeled and measured temperature with boron nitride coated patch. (Solid and dashed lines denote measurements and modeled results, respectively.)

Upon quenching, the BN coating can be easily removed as it dissolves in water, however, transformation of the Al-Si-Fe layer underneath BN coating was a concern. Preliminary microscopic analysis performed on the patched blanks heated in a muffle furnace revealed a fully-formed Al-Si-Fe layer as shown in Figure 29. Nevertheless, a more detailed metallurgical analysis on the coatings of

blanks heated in the roller hearth furnace needs to be carried out, in order to ensure that BN coating is a feasible option in an industrial setting.

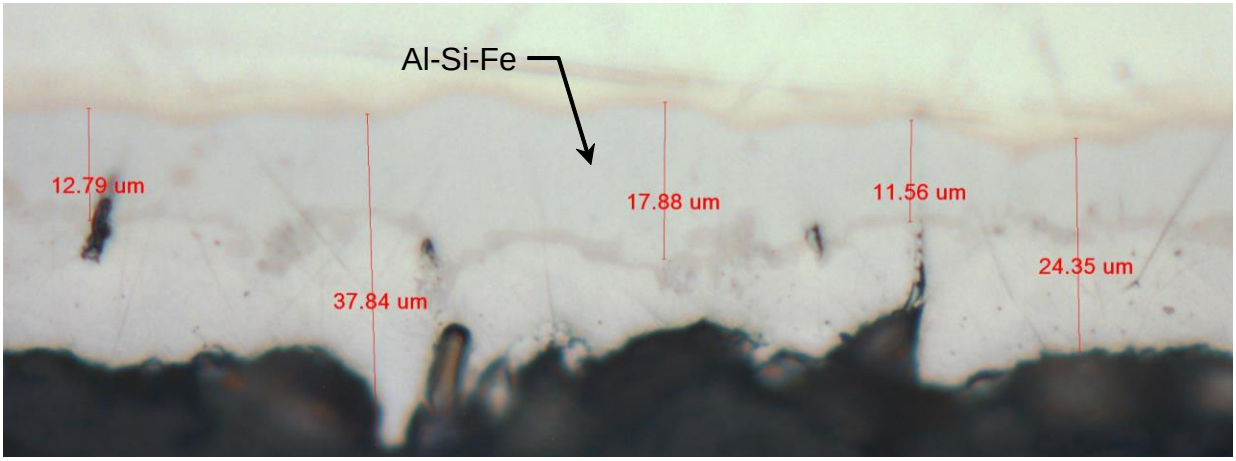

Figure 29: Growth of intermetallic Al-Si-Fe layer in a boron nitride coated patched blank heated in the muffle furnace.

Chapter 5
Conclusion and Future Work

5.1 Conclusions

Models of the heating phase of HFDQ play an important role in ensuring that the UHSS blanks are adequately austenitized, and in the case of Usibor® 1500 P, that the Al-Si coating has transformed into a ternary Al-Si-Fe intermetallic layer having the desired properties and thickness. These models, in turn, require a detailed knowledge of how the sensible and latent energies of the blanks change with heating: while the former is well-known, there is considerable uncertainty regarding the latter.

In this study, an effective specific heat, which accounts for both sensible energy and the latent heat of austenitization, is derived from temperature measurements made on Usibor® 1500 P coupons heated in a muffle furnace. The coupons were first heated to 500°C to avoid introducing uncertainty associated with Al-Si coating transformation and austentization of the substrate 22MnB5 steel. Two techniques were used to model the surrounding temperature: one in which the surrounding temperature is taken to be the steady state temperature of the coupon, and one that is derived from a Monte Carlo radiation model. Both techniques give specific heats that are consistent with that of 22MnB5 below T_{Ac1}.

Next, the influence of austenitization on the effective specific heat was investigated by heating BN-coated 22MnB5 coupons to approximately 900°C in the muffle furnace. The inferred specific heat matches the accepted value for 22MnB5 below T_{Ac1}, and reveals a nonuniform distribution for the latent heat of austentitization between T_{Ac1} and T_{Ac3}. This distribution is also consistent with the power angle recorded when a Gleeble® 3500 thermomechanical simulator is used to heat a Usibor® 1500P coupon according to the same temperature history. Based on these observations and the latent heat of austenitization of 22MnB5, a new $c_{p,eff}$ is proposed that accounts for nonuniform austenitization between T_{Ac1} and T_{Ac3}.

The radiative properties of Usibor® 1500P were then characterized using a near-infrared spectrometer (NIR) and a Fourier transform infrared reflectometer (FTIR). The spectral emissivity measurements made with a near infrared spectrometer on Gleeble-heated Usibor® 1500 P coupons show that, upon melting, ε_λ drops to a value of 0.2 between 900 and 2500 nm. It was assumed that this value extends into the mid-infrared range, thus resulting in a total emissivity of 0.2 at 575°C.

Finally, the characterized thermophysical properties of Usibor® 1500P were used to model the transient blank temperature for blanks heated in both a muffle furnace and a roller hearth furnace. The modeled blank temperatures were within 10% of the blank temperature measured within the furnaces however, measured temperatures showed an increase in the heating rate near 850°C for thicker blanks which was not replicated by the modeled blank temperature. It was observed that the majority of the heat transfer occurring to the blank is via radiation; hence, non-uniform heating within the patch blank can be minimized by painting the patch with a high absorbtant coating to increase the heating rate to the patch. Following this technique, patch blanks were painted with a boron nitride coating, and the measured and modeled heating rate of the patch and the unpatched blank were found to be approximately identical in the muffle furnace. The required heating time for blanks heated in the roller hearth furnace was significantly reduced with the use of a boron nitride coating, although it didn't completely eliminated the non-uniform heating within the blank.

5.2 Future Work

The accuracy of the current model can be further improved by understanding the discrepancy between modeled and measured blank temperatures. A consistent increase in heating rate around 820-850°C is observed in the measured blank temperature that is not reproduced in the modeled temperature. Most likely, the increase in the heating rate at this temperature is caused by either an increase in the absorptivity of the surface or by a decrease in the effective specific heat; for blanks with longer heating times it is possible that the majority of the ferrite is transformed into austenitite by this temperature thus resulting in a lower effective specific heat. It would be possible to determine the amount of austenite formed by performing dilatometry measurements on Gleeble-heated coupons according to the measured temperature history.

Boron nitride coating was investigated in this study as a possible technique to uniformly heat patched blanks; however, the feasibility of this coating in an industrial setting requires further investigation. Specifically, adequate growth of a Al-Si-Fe layer in patches painted with BN coating must be further investigated. Moreover, the impact of using a boron nitride coating on the equipment specifically, quenching dies and furnace rollers must be addressed.

The thermal model developed in this study will be used to derive a coupled thermal-metallurgical model of the HFDQ heating stage that can be used for troubleshooting and process optimization. The temperature profile of the furnace can be optimized to minimize heating time and energy consumption by adjusting zone temperature and roller speed for a variety of different blanks.

Additionally, it will provide useful insight into the heating process that would be helpful to Cosma personnel when evaluating and developing new heating technologies for HFDQ.

Bibliography

[1] J. Aspacher, "Forming Hardening Concepts," in *1st International Conference on Hot Sheet Metal Forming of High-Performance Steel*, Kassel, Germany, 2008.

[2] R. Hund, "Continuous Improvement of Hot Forming Technology," in *3rd International Conference on Hot Sheet Metal Forming of High Performance Steel*, Kassel, Germany, 2011.

[3] H. Karbasian and A. E. Tekkawa, "A Review on Hot Stamping," *Journal of Materials Processing Technology*, vol. 210, pp. 2103-2118, 2010.

[4] P. Åkerstrom, Modelling and Simulation of Hot Stamping, Ph.D Thesis University of Luleå, 2006.

[5] H. Lehmann, "Developments in the Field of Schwarz Heat Treatment Furnaces for Press Hardening Industry," in *3rd International Conference on Hot Sheet Metal Forming of High-Performance Steel*, Kassel, Germany, 2011.

[6] M. G. Twynstra, K. J. Daun, E. F. J. R. Caron, N. Adam and F. and Womack, "Modelling and Optimization of a Batch Furnace for Hot Stamping," in *ASME Summer Heat Transfer Conference*, Minneapolis MN, 2013.

[7] B.-A. Beherens, S. Hübner and M. Demir, "Conductive Heating System for Hot Sheet Metal Forming," in *1st International Conference on Hot Sheet Metal Forming of High Performance Steel*, Kassel, Germany, 2008.

[8] V. Ploshhikin, A. Prihodovsky, J. B. R. Kaiser, H. Linder, C. Lengsdor and K. Roll, "New Heating Technology for the Furnace-Free Press Hardening Process," in *Tools and Technologies for Processing Ultra-High Strength Materials*, Graz, Austria, 2011.

[9] J. N. Rasera, K. J. Daun and M. d'Souza, "Direct Contact Heating for Hot Forming Die Quenching," in *ASME International Mechanical Engineering Congress and Exposition*, Montreal, QC, 2014.

[10] R. Kolleck, R. Veit, H. Hofmann and F.-J. Lenze, "Alternative Heating Concepts for Hot Sheet Metal Forming," in *1st International Conference on Hot Sheet Metal Forming of High-Performance Steel*, Kassel, Germany, 2008.

[11] R. George, A. Bardelcik and M. J. Worswick, "Hot Forming of Boron Steels Using Heated and Cooled Tooling for Tailored Properties," *Journal of Materials Processing Technology*, vol. 212,

no. 11, pp. 2386-2399, 2012.

[12] E. J. Caron, K. J. Daun and M. A. Wells, "Experimental Heat Transfer Coefficient Measurements During Hot Forming Die Quenching of Boron Steel at High Temperatures," *International Journal of Heat and Mass Transfer,* vol. 71, pp. 396-404, 2014.

[13] M. Naderi, Hot Stamping of Ultra High Strength Steels, Ph.D Thesis RWTH Aachen, 2007.

[14] M. J. Holzweißig, A. Andreiev, M. Schaper, J. Lackmann, S. Konrad, C. J. Rüsing and T. Niendorf, "Influence of Short Austenitization Treatments on the Mechanical Properties of Low Alloy Boron Steel," in *5th International Conference on Hot Sheet Metal Forming of High-Performance Steel*, Toronto, Canada, 2015.

[15] C. I. Garcia and A. J. Deardo, "Formation of Austenite in 1.5 pct Mn Steels," *Metallurgical Transactions A,* vol. 12, pp. 521-530, 1981.

[16] E. Radziemska and W. M. Lewandowski, "Heat Transfer by Natural Convection from an Isothermal Downward-Facing Round Plate in Unlimited Space," *Applied Energy,* vol. 68, p. 347, 2001.

[17] K. G. T. Hollands, G. D. Raithby and L. Konicek, "Correlation Equations for Free Convection Heat Transfer in Horizontal Layers of Air and Water," *International Journal of Heat and Mass Transfer,* vol. 18, pp. 879-884, 1975.

[18] G. D. Raithby and K. G. T. Hollands, "Natural Convection," in *Handbook of Heat Transfer Fundamentals*, New York, McGraw-Hill, 1985.

[19] ArcelorMittal, "Properties of Usibor® 1500 P".

[20] M. Naderi, A. Saeed-Akbari and W. Bleck, "The Effects of Non-Isothermal Deformation on Martensitic Transformation in 22MnB5 Steel," *Materials Science and Engineering A,* vol. 487, pp. 445-455, 2008.

[21] S. J. Grauer, E. Caron, N. Chester, M. Wells and K. Daun, "Investigation of Melting in the Al–Si Coating of a Boron Steel Sheet by Differential Scanning Calorimetry," *Journal of Materials Processing Technology,* vol. 216, p. 89–94, 2014.

[22] D. F. Watt, L. Coon, B. Bibby, J. Goldak and C. Henwood, "An Algorithm for Modelling Microstructural Development in Weld-Affected Zones (PartA) Reaction Kinetics," *Acta Metallurgica,* vol. 36, pp. 3029-3035, 1988.

[23] J. Tonne, J. Clobes, M. Alsmann, A. Ademaj, M. Mischka, W. Morgenroth, H.-H. Becker and O.

Stursburg, "Model-based Optimization of Furnace Temperature Profiles with Regard to Economic and Ecologic Aspects in Hot Stamping of 22MnB5," in *4th International Conference on Hot Sheet Metal Forming of High Performance Steel*, Lulea, Sweden, 2013.

[24] C. Balea, E. Bélislea, P. Chartranda, S. Decterova, G. Eriksson, K. Hackb, I.-H. Junga, Y.-B. Kanga, J. Melançona, A. Peltona, C. Robelina and S. Petersen, "FactSage thermochemical software and databases — recent developments," *Calphad*, vol. 33, p. 295–311, 2009.

[25] Z.-K. Liu and Y. A. Chan, "Thermodynamic Assessment of the Al-Fe-Si System," *Metallurgical and Materials Transactions A*, vol. 30A, pp. 1081-1095, 1999.

[26] N. L. Chester, K. J. Daun and M. A. Wells, "Experimental Measurements of Spectral Emissivity of Al-Si Coated Steel Blanks undergoing Rapid Heating," in *ASME International Mechanical Engineering Congress and Exposition*, Montreal, 2014.

[27] A. V. Tikhonov and V. I. Arsenin, Solutions of Ill-posed Problems, Washington DC: Winston and Sons, 1977.

[28] P. C. Hansen, Rank-Deficient and Discrete Ill-Posed Problems: Numerical Aspects of Linear Inversion, Philadelphia: SIAM, 1999.

[29] M. F. Modest, Radiative Heat Transfer, 3rd Ed., New York: Academic Press, 2013.

[30] G. P. Krielaart, C. M. Brakman and S. Zwaag, "Analysis of Phase Transformation in Fe-C Alloys using Differential Scanning Calorimetry," *Journal of Materials Science*, vol. 51, pp. 1501-1508, 1996.

[31] T. L. Bergman, A. S. Lavine, F. P. Incopera and D. P. Dewitt, Fundamentals of Heat and Mass Transfer, Seventh ed., New Jersey: John Wiley & Sons, 2011.

[32] J. Wilsius, B. Tavernier and D. Abou-Khalil, "Experimental and Numerical Investigation of Various Hot Stamped B-pillar Concepts Based on Usibor 1500P," in *3rd International Conference on Hot Sheet Metal Forming of High-Performance Steel*, Kassel, Germany, 2011.

Appendix A
Sensitivity Analysis

In this section, the sensitivity of the modeled temperature of the bumper and hinge pillar blanks due to the variations in T_{surr}, air gap thickness, and α at the melting temperature of Al-Si layer is assessed. There is some uncertainty associated with these parameters due to the assumptions made during the development of the heat transfer model. The sensitivity analysis for the modeled temperature of b-pillar blanks is omitted as it does not vary significantly from the hinge pillar blanks. The variation in the surrounding temperature results in the largest uncertainty in the modeled temperature.

Surrounding Temperature

Based on the temperature control strategy used in the roller hearth furnace, radiant tubes in each zone are turned on/off if the measured zone temperature differs from the set-point temperature by more than 20°C. During a production environment, zone temperature can be ±20°C of the set-point temperature and the effect of this range in surrounding temperature is assessed by modeling the temperature of the bumper and hinge pillar blanks with each zone set-point temperature set to its maximum (set-point temperature + 20°C) and minimum value (set-point temperature – 20°C) as shown in Figure 30. The modeled temperature of both bumper and hinge pillar blanks varies significantly with the maximum uncertainty of 10% and an average uncertainty of 5% due to the variation in the surrounding temperature.

Air Gap Thickness

In the heat transfer model, the air gap thickness between the patch and the substrate blank was assumed to be constant 0.1mm; however, the thickness of the air gap varies considerably and is largely dependent on the size of the patch and the number of spot-welds. The air gap thickness is zero at the spot-welds and increases significantly further from the spot-welds. Blanks with identical radiative properties for both patch and substrate blank experience identical heating, thus, there is negligible conduction occurring between the patch and the substrate blank. In this case, the air gap thickness has negligible effect on the modeled temperature, however, this effect is considerable when modeling blank temperature of patches coated with boron nitride coating. Figure 31 shows an average uncertainty of 5% in the modeled temperature of the boron nitride coated patch of the hinge pillar blank when the air gap thickness is varied from 0.005 to 0.500 mm.

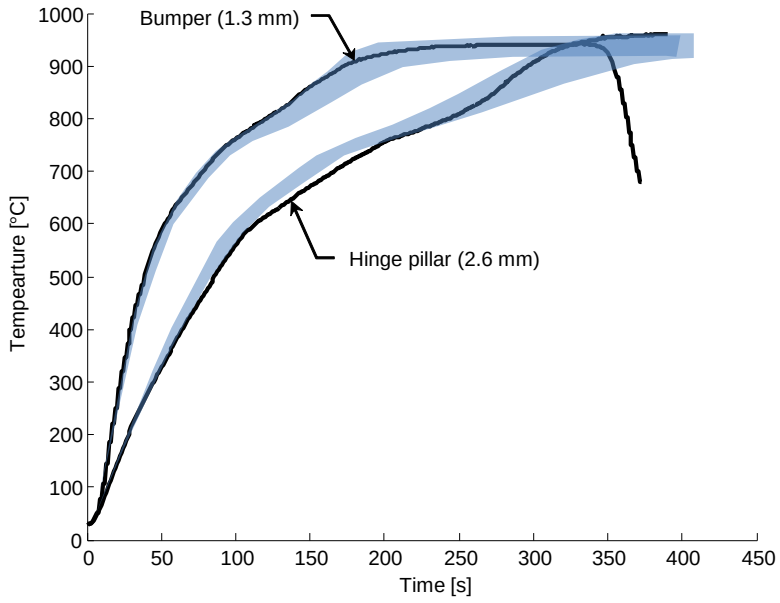

Figure 30: Shows modeled temperature range calculated based on the upper and lower limits of surrounding temperature in each zone.

Absorbtivity of Usibor® 1500 P at 575°C

The radiative properties of Usibor® 1500 P were calculated using NIR spectrometer and FTIR reflectometer. However, since the FTIR measurements could not be performed between 575 to 700°C, the total absorbtivity of Usibor® 1500 P at 575°C was assumed to be 0.2 based solely on the NIR spectrometer measurements. Figure 32 shows the variation in the modeled temperature with maximum variation of 4% as α is varied from 0.15 to 0.25 at 575°C.

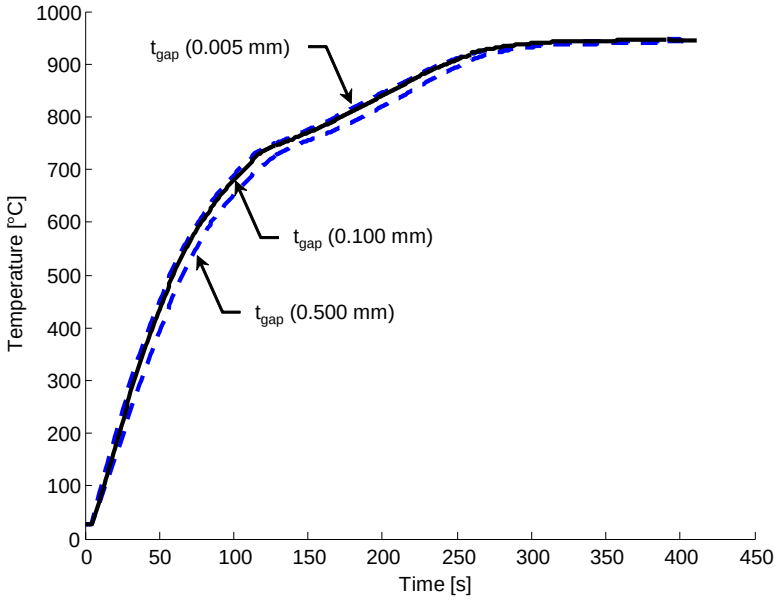

Figure 31: Shows the modeled temperature of the boron nitride coated hinge pillar patch with different air gap thicknesses.

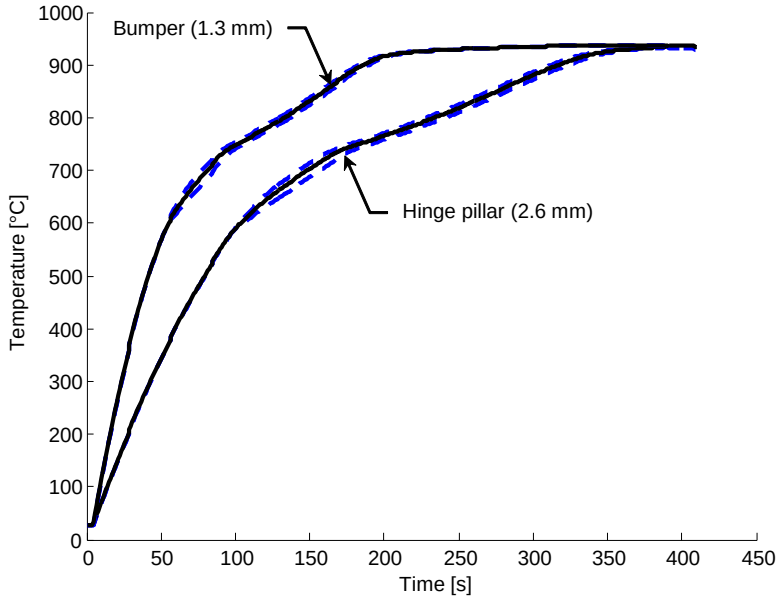

Figure 32: Shows the modeled temperature of the bumper (1.3mm) and hinge pillar (2.6mm) blanks with α at 575°C set to 0.15, 0.2 and 0.25. (Solid lines show the modeled temperature with α set to 0.2 and dashed lines show the modeled temperature with α set to 0.15 and 0.25)